TU Delft

Delft University of Technology

Document Version
Final published version

Citation (APA)
Gonzalez Silva, J., Ferrari, R., & van Wingerden, J. W. (2025). Towards Control of Large-Scale Wind Farms: A Multi-rate Distributed Control Approach. In C. Ocampo-Martinez, & N. Quijano (Eds.), *Energy Systems Integration for Multi-Energy Systems : From Operation to Planning in the Green Energy Context* (pp. 261-294). (Green Energy and Technology; Vol. Part F336). Springer. https://doi.org/10.1007/978-3-031-69015-0_11

Important note
To cite this publication, please use the final published version (if applicable).
Please check the document version above.

Copyright
In case the licence states “Dutch Copyright Act (Article 25fa)”, this publication was made available Green Open Access via the TU Delft Institutional Repository pursuant to Dutch Copyright Act (Article 25fa, the Taverne amendment). This provision does not affect copyright ownership.
Unless copyright is transferred by contract or statute, it remains with the copyright holder.

Sharing and reuse
Other than for strictly personal use, it is not permitted to download, forward or distribute the text or part of it, without the consent of the author(s) and/or copyright holder(s), unless the work is under an open content license such as Creative Commons.

Takedown policy
Please contact us and provide details if you believe this document breaches copyrights.
We will remove access to the work immediately and investigate your claim.

This work is downloaded from Delft University of Technology.

Green Open Access added to TU Delft Institutional Repository

'You share, we take care!' - Taverne project

https://www.openaccess.nl/en/you-share-we-take-care

Otherwise as indicated in the copyright section: the publisher is the copyright holder of this work and the author uses the Dutch legislation to make this work public.

Towards Control of Large-Scale Wind Farms: A Multi-rate Distributed Control Approach



Jean Gonzalez Silva, Riccardo Ferrari, and Jan-Willem van Wingerden

1 Introduction

With the increasing share of wind energy in the generation mix, concerns regarding ensuring power system stability are ever more relevant due to wind variability, and have been accompanied by discussions to address this yet unresolved issue [1]. In this regard, technological advancements will be required to tackle these challenges. In the context of wind farms (WF), further research must be pursued towards the development of control algorithms, to allow WF owners to meet the requirements posed by future regulations. The regulations are evolving to ensure seamless integration of WFs into power grids [2–4]. One major change is posed by altering the main objective of WF control: moving from power maximization to power tracking. Indeed, active power tracking controllers [5–7] allow WF operators to offer tracking capabilities that are closer to those of conventional energy sources, being able to provide ancillary services to the grid [8], such as frequency regulation [9, 10]. In addition to this, power tracking controllers can be designed to simultaneously achieve secondary objectives, such as balancing structural loading across WFs [11, 12], thus permitting WF operators to enhance their resource management. Current challenges include not only the shift paradigm from maximization to tracking but also moving from centralized to distributed control for large-scale WF applications. The latter challenge stems from the substantial quantity of wind turbines (WTs), making it unfavorable to transmit and receive information within a single node. Ben-

J. Gonzalez Silva (✉) · R. Ferrari · J.-W. van Wingerden
Delft Center for Systems and Control, Delft University of Technology, 2628CD Delft, The Netherlands
e-mail: J.GonzalezSilva@tudelft.nl

R. Ferrari
e-mail: R.Ferrari@tudelft.nl

J.-W. van Wingerden
e-mail: J.W.vanWingerden@tudelft.nl

© The Author(s), under exclusive license to Springer Nature Switzerland AG 2025

C. Ocampo-Martinez and N. Quijano (eds.), *Energy Systems Integration for Multi-Energy Systems*, Green Energy and Technology, https://doi.org/10.1007/978-3-031-69015-0_11

efiting from the current turbine hardware, our proposed distributed controller can be implemented in the individual WTs and solve WF objectives by communicating only with neighbors. In this way, it reduces installation costs by eliminating the need for a supervisory or central control system operating point.

1.1 WF Control: A Centralized Approach and Its Reliance on Wake Modeling

The design of centralized WF controllers has been proposed by several researchers [13–17] and tested, although still focusing on power maximization, in the field [18, 19]. As a WT extracts energy from the wind, it reduces the downstream wind velocity and adds turbulence to the flow. The altered flow is called the wake of a WT. Under the wake, downstream WTs suffer from insufficient energy availability and additional loads. When they are not capable of producing the required amount of power, i.e., the maximum power that can be produced is below the reference level set, we have the so-called turbine *saturation*, which is explored in this work as a consequence of severe waked conditions. In addition, the presence of wakes can lead to significant variations in structural loads across the WF [20].

To mitigate these issues through control design, engineers and researchers have modeled the wind farm with analytical steady-state models. Unsuccessfully, these models have demonstrated low accuracy through the validation by measurement data, as reported in [19]. The accurate modeling of wake effects is a nontrivial task to achieve because of the flow's dynamic time-varying nature and uncertainty, for instance, caused by changes in atmospheric stability. The reliance on a wake model is therefore compromised. However, when considering WF controllers, it becomes crucial to account for the wind flow interactions between WTs [21].

1.2 The Shift from Centralized to Distributed WF Controllers

The implementation of centralized controllers in large-scale systems poses some challenges with the increased complexity of the network, such as network topology constraints, communication overhead, and computation effort [22]. Moreover, centralized approaches are susceptible to a single point of failure and often lack the flexibility to include new agents or remove failed ones without redesigning the controller, making them unsuitable for plug-and-play solutions. Therefore, centralized controllers for large-scale WFs lack scalability. In particular, challenges in WF communication arise due to a large number of involved WTs. Management of transmitting and receiving information from hundreds of WTs in a single node at a required rate is unfavorable. In addition, the computation effort required by controllers of large-scale WFs can be significantly high, as observed in some optimal controllers [15, 23, 24].

One way to circumvent these issues is to implement distributed control approaches, where networked local controllers manage parts of the farm. In this way, the mentioned communication and computation issues are solved by achieving *modularity* and *sparsity*.

Modularity Defined as the property of a controller where all update laws are identical. Each WT or cluster of WTs only needs to know which WTs or clusters to communicate with.

Sparsity Referred to the property that adding or removing a single WT or a cluster of WTs from operation does not affect the computational effort of WTs that are not in their vicinity.

From an economic standpoint, distributed control is advantageous for the deployment and implementation of controllers on large-scale systems. This solution does not require all-to-all communication or a central computational unit, and it introduces WTs to the market equipped with localized controllers responsible for achieving WF goals. The expenses associated with employing a WF controller can be significantly diminished, albeit with potential implications for the reliability of power generation in existing distributed controllers.

1.3 Existing Literature on Distributed Controllers

The future outlook for WF control envisions a shift toward decentralization, resembling the applications seen in micro-grid [25, 26] and power systems [27, 28]. In [29] and [24], the authors propose algorithms that integrate the contribution of building energy systems with charging stations to the grid in a distributed manner. In [27, 28], the authors proposed controllers for power systems going from a fully decentralized to a distributed control that results in an improvement in oscillation damping. Moreover, robustness against failures can be enhanced with distributed methods [30], in which local failures can also be easily detected [31] and compensated for.

Among the first works towards distributed control in WFs are the ones from Marden et al. [32] and Gebraad et al. [33], where the WT actions take into consideration their neighbors. Avoiding a centralized controller, [34, 35] maximize power production of the wind power plant using data-driven and learning approaches. In [36], the authors estimate the wind speed direction using an average consensus algorithm. Finally, coalitional control, a strategy where controllers are temporarily clustered into alliances, so-called *coalitions*, to jointly achieve a control objective [22], was applied in [23] for WF control. Also, clusters of turbines are identified in [37], which hinges on the correlation observed in the measured power signals, for yaw control.

1.4 Our Contributions

In this work, we design a distributed WF controller to achieve the following objectives:

1. Regulate the WF's active power generation to a time-varying set point as required;
2. Distribute the power references efficiently across the sparse WF communication network;
3. Achieve aerodynamic load balancing as a surrogate for structural loading.

Aiming to reach central performance as an extension of [17], the proposed framework makes use of a multi-rate scheme [38, 39] to compute the average consensus [40, 41] before performing the control actions. Hence, we term this framework as the Multi-rate Consensus-based Distributed Control (MCDC).

Particularly, to achieve each of the aforementioned objectives, the MCDC first compensates cooperatively for the power losses. The power losses stem from low wind availability, for instance, coming from wake effects, where interactions among WTs disrupt the ability of individual WTs to attain their specific references. The rationale behind the power compensation is that those WTs with excess available power can provide additional energy extraction to achieve WF-level reference tracking. The power losses are estimated using the available WT data, where the average across the WF network is obtained at a higher sampling rate than the rate at which compensation takes place. By reaching the average consensus on the power losses, the compensation process is distributed across the entire WF and executed by those WTs that have sufficient wind resources. Then, a leader-follower consensus algorithm is utilized to distribute the global power reference throughout all WTs, solving the so-called alignment problem [40]. Finally, we balance the aerodynamic loads of the WTs across the WF in the same fully distributed manner, where the average of the aerodynamic loads is obtained with average consensus. Through the reduction of aerodynamic load variability, the WF's available power is increased compared to a uniform distribution of power, as demonstrated in [12]. The authors have shown that by implementing thrust force balancing, turbine *saturation* is avoided. Furthermore, the balancing of aerodynamic loads, as a surrogate model of structural loads, results in a uniform degradation of WTs.

The main contributions of this work encompass the development of the proposed MCDC framework, including stability analysis, and its comparison with centralized control and the distributed approach adapted from [42–44]. The MCDC framework demonstrates to possess the following main advantages:

1. The proposed WF control, MCDC, does not rely on explicitly modeling WT interaction;
2. The MCDC is distributed and computationally tractable, making it straightforward to implement;
3. The performance of the MCDC is comparable with the centralized controller albeit achieved with a fully distributed methodology.

By presenting these advantages, the study underscores the effectiveness and potential of the MCDC framework as a distributed control approach in WFs. The achieved flexibility and applicability for large-scale farms offered by the proposed control system present a promising solution for integrating wind energy into the electricity grid and multi-energy systems. We contribute to a more sustainable and resilient energy system by improving power tracking capability and leveraging distributed communication.

1.5 Outline of the Remainder of the Chapter

The structure of this chapter is: First, the distributed WF control problem will be formulated in Sect. 2. Second, the proposed distributed control, namely MCDC, for power compensation, power distribution, and thrust balance is presented in Sect. 3. In Sect. 4, simulation results will be presented using a high-fidelity simulator to evaluate the proposed controller. Lastly, conclusions and future works will be discussed in Sect. 6.

2 Problem Formulation

In this section, we formulate the distributed WF control problem by first presenting the considered model, followed by the WF control objectives and existing centralized design, and, finally, the assumption for the application of distributed control.

2.1 Wind Farm Model

We model the WF as a linear time-invariant dynamic system, composed of n WTs. Although WT open-loop dynamics are non-linear, each turbine is equipped with its own *local* feedback controller designed to track a local reference power set point. The closed-loop behavior of each WT is then modeled to be linear. The WT controller employs both blade pitching and generator torque to regulate the power generation, as presented in [17].

Considering the step response of generator power and thrust force to the power reference (see Fig. 1), the following generator power model is identified from the closed-loop WT behavior utilizing system identification:

$$P_{\mathrm{g},i}(k+1) = a_{\mathrm{P}} P_{\mathrm{g},i}(k) + b_{\mathrm{P}} P_{\mathrm{g},i}^{\mathrm{ref}}(k) + q_{\mathrm{P},i}(k), \tag{1}$$

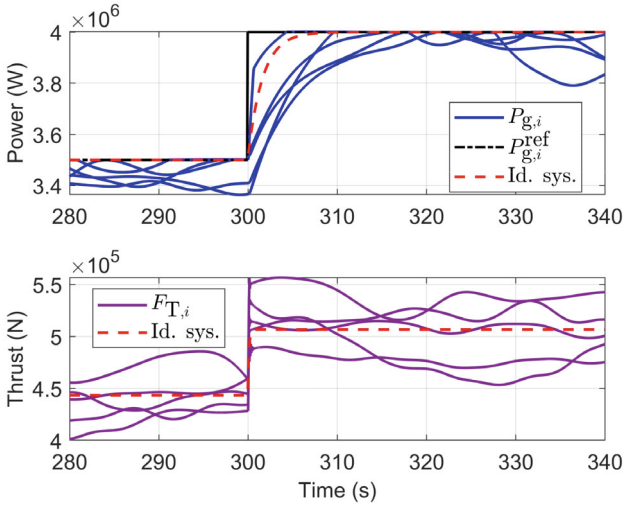


Fig. 1 Multiple realizations of the power and thrust force response when a step is applied to the power reference with a turbulent inflow. The power and thrust force response of the identified model is depicted

where k is the time step; $P_{g,i}$ and $P^{ref}_{g,i}$ are the power output and power reference of turbine i, respectively; a_P and $b_P \in \mathbb{R}^+$ are identified parameters from simulations of WTs with their local feedback controller for power tracking; $q_{P,i}(k)$ represents the power discrepancies caused by model mismatch and possible *saturation* of turbine i, which occurs due to low available wind conditions, often caused by the wakes of neighbor WTs. Seeking simplicity, we utilize a first-order representation focusing on the dominant transient response, being a_P and b_P scalars. The use of high-order models, i.e., replacing the scalar parameters with matrices, requires only minor extensions with appropriate notation.

Similarly, we identify the model of the thrust force $F_{T,i}$ acting on the i-th WT as a first-order dynamical model:

$$F_{T,i}(k+1) = a_T F_{T,i}(k) + b_T P^{ref}_{g,i}(k) + q_{T,i}(k), \tag{2}$$

where a_T and $b_T \in \mathbb{R}^+$ are identified parameters; and $q_{T,i}(k)$ represents the discrepancies of thrust force given a low wind availability and the power reference $P^{ref}_{g,i}$. Given (1) and (2), each WT is represented as a dynamic system where the power reference serves as the input and the generator power along with thrust force as the output. The choice of the first-order models is driven by our focus on the dominant transient characteristics to design the WF controller. Conservatively, the proposed WF controller incorporates an integral term, imparting robustness to fluctuations in system parameters, as seen in [45, 46].

At the wind farm level, there exists a substantial temporal distinction between the dynamics of WTs with the power tracking controller, typically designed at sampling time ranging from 0.00125–0.1 s with a response time of 5–10 s, and the dynamics of wake interactions, of 100–300 s, contingent upon the turbine spacing and wind speed. In our study case, with the average wind inflow of 10 ms^{-1}, the rise time of the power tracking controller is about 8 s, while wake propagation spans between 120 and 225 s. Due to this time-scale separation between the WT dynamics and the wake flow dynamics, we make the following assumption:

Assumption 1 (*Decoupled WF model among WTs*) Models (1) and (2) for WT i are uncoupled with any other WT.

The disturbance signals $q_{\mathrm{P},i}$ and $q_{\mathrm{T},i}$ not only represent unmodelled behaviors, such as the effects from the turbulence in the flow, but they also stem from the effects of the slow time-scale wake interaction. Moreover, the signals $q_{\mathrm{P},i}(k)$ and $q_{\mathrm{T},i}(k)$ incorporate turbine *saturation* when it occurs [47].

By combining the dynamical models for n WTs and considering Assumption 1, we thus obtain the following multi-input and multi-output (MIMO) WF model:

$$\begin{bmatrix} P_{\mathrm{g},1}(k+1) \\ \vdots \\ P_{\mathrm{g},n}(k+1) \\ F_{\mathrm{T},1}(k+1) \\ \vdots \\ F_{\mathrm{T},n}(k+1) \end{bmatrix} = \left[\begin{array}{c|c} A_{\mathrm{P}} & 0_{n\times n} \\ \hline 0_{n\times n} & A_{\mathrm{T}} \end{array}\right] \begin{bmatrix} P_{\mathrm{g},1}(k) \\ \vdots \\ P_{\mathrm{g},n}(k) \\ F_{\mathrm{T},1}(k) \\ \vdots \\ F_{\mathrm{T},n}(k) \end{bmatrix} + \begin{bmatrix} B_{\mathrm{P}} \\ B_{\mathrm{T}} \end{bmatrix} \begin{bmatrix} P^{\mathrm{ref}}_{\mathrm{g},1}(k) \\ \vdots \\ P^{\mathrm{ref}}_{\mathrm{g},n}(k) \end{bmatrix} + \begin{bmatrix} q_{\mathrm{P},1}(k) \\ \vdots \\ q_{\mathrm{P},n}(k) \\ q_{\mathrm{T},1}(k) \\ \vdots \\ q_{\mathrm{T},n}(k) \end{bmatrix}, \tag{3}$$

where $A_{\mathrm{P}} := \mathrm{diag}(a_{\mathrm{P}})$, $B_{\mathrm{P}} := \mathrm{diag}(b_{\mathrm{P}})$, $A_{\mathrm{T}} := \mathrm{diag}(a_{\mathrm{T}})$, and $B_{\mathrm{T}} := \mathrm{diag}(b_{\mathrm{T}})$ are $n \times n$ matrices.

2.2 Wind Farm Control

The WF control has as its objectives to compensate for power tracking losses due to low wind availability and to balance thrust forces across the WF. In this section, we present a solution to achieve these objectives using feedforward and feedback strategies. From our previous discussion on the WT modeling, the generator power reference $P^{\mathrm{ref}}_{g,i}$ acts as the sole input to the i-th WT, and it is set as

$$P^{\mathrm{ref}}_{\mathrm{g},i}(k) = \hat{P}^{\mathrm{ref}}_{\mathrm{g},i}(k) + u_i(k), \tag{4}$$

where the term $u_i(k)$ is the feedback term utilized to compensate for power tracking errors and to balance thrust forces across the WTs; while $\hat{P}^{\mathrm{ref}}_{\mathrm{g},i}(k)$ is the feedforward

term, being the desired power reference for each WT. Notice that there is a degree of freedom in assigning the feedforward signals, as long as their sum is the total wind farm power reference.

Given that there are two different goals for the feedback, $u_i(k)$ is defined as

$$u_i(k) = u_{\mathrm{P},i}(k) + u_{\mathrm{T},i}(k), \tag{5}$$

where $u_{\mathrm{P},i}(k)$ is designed for power compensation and $u_{\mathrm{T},i}(k)$ for balancing thrust forces. Following the electro-mechanical constraint of typical turbines, the power reference signal (4), as the input of the WTs, is saturated as

$$P_{\mathrm{g},i}^{\mathrm{ref}}(k) = \begin{cases} 0 & \text{if } P_{\mathrm{g},i}^{\mathrm{ref}}(k) \leq 0 \\ P_{\mathrm{g},i}^{\mathrm{ref}}(k) & \text{if } 0 < P_{\mathrm{g},i}^{\mathrm{ref}}(k) \leq P_{\mathrm{g},i}^{\mathrm{rated}} \\ P_{\mathrm{g},i}^{\mathrm{rated}} & \text{otherwise} \end{cases} \tag{6}$$

where $P_{\mathrm{g},i}^{\mathrm{rated}}$ is the rated power of turbine i.

Centralized Controller

The controller proposed in [17] is a centralized solution to reach power compensation and thrust force balancing. There, an integral control is used for the power compensation, such that

$$u_{\mathrm{P},i}(k) = u_{\mathrm{P},i}(k-1) + K_{\mathrm{P}}\mathbf{1}_{1\times n}e_{\mathrm{P}}(k), \tag{7}$$

where K_{P} is a scalar integrator gain for the power compensation, $\mathbf{1}_{1\times n}$ is the row vector with all elements equal to one, and $e_{\mathrm{P}}(k) = [e_{\mathrm{P},1}(k), e_{\mathrm{P},2}(k), ..., e_{\mathrm{P},n}(k)]^{\intercal}$ a vector containing the power tracking errors of each WT,

$$e_{\mathrm{P},i}(k) = \hat{P}_{\mathrm{g},i}^{\mathrm{ref}}(k) - P_{\mathrm{g},i}(k), \tag{8}$$

where the superscript $\intercal$ denotes transpose.

The wind-farm-wide power tracking error is the aggregation of all WT-level errors, i.e., $e_{\mathrm{P}}^{\mathrm{total}}(k) = \mathbf{1}_{1\times n}e_{\mathrm{P}}(k) = \sum_{i=1}^{n}\left(\hat{P}_{\mathrm{g},i}^{\mathrm{ref}}(k) - P_{\mathrm{g},i}(k)\right)$, information necessary for computing (7).

Similarly, an integral control is used for aerodynamic load balancing

$$u_{\mathrm{T},i}(k) = u_{\mathrm{T},i}(k-1) + K_{\mathrm{T}}e_{\mathrm{T},i}(k), \tag{9}$$

where K_{T} is a scalar integrator gain for the thrust balance and

$$e_{\mathrm{T},i}(k) = F_{\mathrm{T}}^{\mathrm{avg}}(k) - F_{\mathrm{T},i}(k) \tag{10}$$

is the thrust force error between the average of the thrust forces across the WF $F_{\mathrm{T}}^{\mathrm{avg}}$ and the thrust force $F_{\mathrm{T},i}$ acting on WT i. To compute $F_{\mathrm{T}}^{\mathrm{avg}}$ the information of all thrust forces is required for computing (9).

In the vector form, we define the average matrix $\mathrm{W}_{\mathrm{avg}} = \frac{1}{n}\mathbf{1}_{n\times 1}\mathbf{1}_{1\times n}$ and rewrite (7) and (9), such that

$$u_{\mathrm{P}}(k) = u_{\mathrm{P}}(k-1) + \bar{K}_{\mathrm{P}} n \mathrm{W}_{\mathrm{avg}} e_{\mathrm{P}}(k), \tag{11}$$

where $u_{\mathrm{P}}(k) = [u_{\mathrm{P},1}(k), u_{\mathrm{P},2}(k), ..., u_{\mathrm{P},n}(k)]^{\intercal}$ and $\bar{K}_{\mathrm{P}} = \mathrm{diag}(K_{\mathrm{P}})$; and

$$u_{\mathrm{T}}(k) = u_{\mathrm{T}}(k-1) + \bar{K}_{\mathrm{T}}\left(\mathrm{W}_{\mathrm{avg}} - I_n\right) F_{\mathrm{T}}(k), \tag{12}$$

where $u_{\mathrm{T}}(k) = [u_{\mathrm{T},1}(k), u_{\mathrm{T},2}(k), ..., u_{\mathrm{T},n}(k)]^{\intercal}$, $F_{\mathrm{T}}(k) = [F_{\mathrm{T},1}(k), F_{\mathrm{T},2}(k), ..., F_{\mathrm{T},n}(k)]^{\intercal}$, $\bar{K}_{\mathrm{T}} = \mathrm{diag}(K_{\mathrm{T}})$, and I_n is the identity matrix of order n. Notice that the average power tracking error vector $\mathrm{W}_{\mathrm{avg}} e_{\mathrm{P}}$ and the average thrust force vector $\mathrm{W}_{\mathrm{avg}} F_{\mathrm{T}}$ contain the information of all WT at each their elements.

2.3 Wind Farm Network

The centralized controller from Sect. 2.2 requires the information of the entire WF to compute the feedback terms, consisting of (7) and (9). Moving towards distributed architectures, WTs no longer require the overall WF information, instead, they require communication with their neighbors' WTs. In this section, we introduce some preliminaries on graph theory, used in our design, as well as a critical assumption on the communication network linking WTs in the WF.

A graph $\mathcal{G}$ is defined as $\mathcal{G} = (\mathcal{V}, \mathcal{E})$, where $\mathcal{V} = v_1, ..., v_n$ is its vertex set, with $|\mathcal{V}| = n$ the number of agents, and $\mathcal{E} \subseteq \mathcal{V} \times \mathcal{V}$ its edge set. $\mathcal{L}$ is the Laplacian matrix, defined by $\mathcal{L} = \mathcal{D} - \mathcal{A}$, where $\mathcal{D} = \mathrm{diag}(d_1, ..., d_n)$ is the in-degree matrix and $\mathcal{A}$ is the adjacency matrix. The diagonal elements $l_{i,j}$ of $\mathcal{L}$ are therefore equal to the in-degree of vertex v_i, and the off-diagonal elements $l_{i,j}$ are -1 if there is an edge from vertex v_i and v_j, or 0 otherwise. The open neighborhood of v_i is defined by the set of neighbors $\mathcal{N}_i$ containing all the adjacent vertices to v_i excluding itself. A graph $\mathcal{G}$ is said to be undirected if $e_{ij} \in \mathcal{E}$ implies $e_{ji} \in \mathcal{E}$. An undirected graph, then, is said to be connected if for each vertex, there exists an edge between it and at least one other vertex.

A communication network in a wind farm induces a graph $\mathcal{G}$ which shares the same topology, i.e., for two vertices $v_i, v_j \in \mathcal{V}$ there exists an edge between them if the two can exchange information. We assume the following.

Assumption 2 (*Connected network*) The communication network is such that the induced graph $\mathcal{G}$ is undirected and connected.

By Assumption 2, any two distinct vertices of the graph $\mathcal{G}$ are connected through a path, meaning that there is always a directed spanning tree from a vertex to all other vertices in the graph. This assumption ensures that every agent can reach average consensus [41] and that the leader-follower consensus converges [40].

3 Multi-rate Consensus-Based Distributed Control

We propose the so-called Multi-rate Consensus-based Distributed Control (MCDC). The MCDC aims to effectively counteract power losses mainly attributed to wake effects and to achieve balance in thrust forces across the WF in a distributed manner. To reduce the communication efforts while still attaining performance levels akin to centralized controllers, the WTs are suggested to engage in communication with a constrained range to estimate the entire WF information. This involves utilizing an average consensus algorithm to estimate average power losses and average thrust forces, from which feedback signals are computed. Employing a multi-rate strategy, the proposed distributed framework demonstrates performance comparable to centralized controllers in the numerical simulations.

The scheme consists of three control components: a power compensator, a power distributor, and a thrust balancer. The overall proposed distributed WF control is depicted in Fig. 2. The core idea is to reach consensus on the relevant WF state estimates within each control component between their sampling times, utilizing only neighborhood information. This approach substantially reduces the complexity and resource requirements of the WF communication network. Then, these estimates are utilized to compute the power reference for each turbine.

The remainder of this section is organized as follows. First, we present the average consensus conducted between samplings in Sect. 3.1. Then, in Sect. 3.2, we present the cooperative power compensation utilizing a calculated average of power loss. The

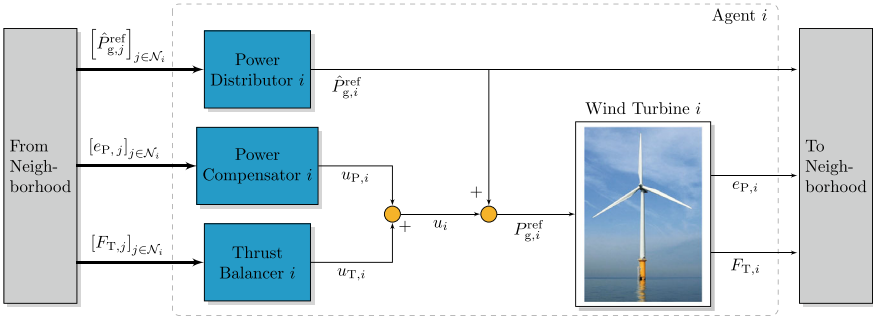


Fig. 2 Block diagram of the distributed control scheme. At each agent i, there is a power distributor, a power compensator, and a thrust balancer that provides the power reference for WT i. Bold arrows represent vectors of signals from the neighborhood $\mathcal{N}_i$, distinguishing from the scalar ones

power compensation is followed by the power distribution in Sect. 3.3, presented in a fully distributed manner. Finally, the distributed thrust force balance is presented in Sect. 3.4.

3.1 Average Consensus Within the Wind Farm Control Sampling Time

Our proposed multi-rate controller employs average consensus algorithms [40, 41] conducted at a higher sampling rate than the WF control action's execution rate. This design consideration is in line with the control of power systems, where different time scales are accounted for [42]. The WF control typically operates at a low time scale, particularly between 20 s and 10 min [10], being suitable for conducting consensus algorithms to estimate the relevant WF information within the sampling time of the WF control.

In this subsection, we present a general formulation of the consensus algorithm, which is utilized to obtain the estimates for the power compesator and thrust balancer. The average consensus of a state $x \in \mathbb{R}^n$, is to be achieved at each WT within $h \in \mathbb{N}$ iterations, the consensus horizon. For clarity, the average consensus algorithm is divided into three stages: *(re-)initialization*; *inner iteration*; and *final assignment*.

In the *(re-)initialization*, the state variable of the average consensus, x_i^{avg} is initialized as

$$x_i^{\text{avg}}(0) = x_i(k). \tag{13}$$

Then, the *inner iteration* is recursively conducted over the consensus horizon, as follows:

$$x_i^{\text{avg}}(c+1) = w_{i,i} x_i^{\text{avg}}(c) + \sum_{j \in \mathcal{N}_i} w_{i,j} x_j^{\text{avg}}(c), \tag{14}$$

for $c \in \{0, 1, \ldots, h-1\}$, where $w_{i,i}$ is the weight on x_i^{avg} at vertex i, and $w_{i,j}$ are the weights on x_j^{avg} at vertex i. As the last stage, the *final assignment* is

$$x_i^{\text{avg, final}}(k|k+1) = x_i^{\text{avg}}(h), \tag{15}$$

where $x_i^{\text{avg, final}}$ is the final average value obtained after h steps and utilized for defining the WF control action. The notation $(k|k+1)$ is utilized to highlight that the estimate of the average of $x(k)$ can only be obtained at $k+1$.

By setting $w_{i,j} = 0$ for $j \notin \mathcal{N}_i$, we can then rewrite (13)–(15) in a vector form

$$x^{\text{avg}}(0) = x(k), \tag{16a}$$

$$x^{\text{avg}}(c+1) = W x^{\text{avg}}(c), \forall c \in \{0, 1, ..., h-1\} \tag{16b}$$

$$x^{\text{avg, final}}(k|k+1) = x^{\text{avg}}(h), \tag{16c}$$

where $W = [w_{i,j}]$ is the average consensus weight matrix. The matrix W is structured to respect the communication topology and has to satisfy the following conditions:

$$\lambda_1(W) = 1 \text{ and } |\lambda_i(W)| \leq 1 \text{ for all } i = 2, \ldots, n, \tag{17a}$$

$$W\mathbf{1}_{n\times 1} = \mathbf{1}_{n\times 1}, \tag{17b}$$

$$\mathbf{1}_{n\times 1}^{\mathsf{T}} W = \mathbf{1}_{n\times 1}^{\mathsf{T}}. \tag{17c}$$

While average consensus is only reached in the limit, a suitable value can be achieved in finite iterations, by choosing a sufficiently large h. Moreover, the optimal design of W to achieve the fastest convergence and enhance accuracy is obtained by solving the following optimization problem, the so-called Fastest Discrete-Time Consensus problem [48]:

$$\underset{w_{ij}}{\text{minimize}} \quad \rho\left(W - (1/n)\mathbf{1}_{n\times 1}\mathbf{1}_{n\times 1}^{\mathsf{T}}\right) \tag{18a}$$

subject to

$$W\mathbf{1}_{n\times 1} = \mathbf{1}_{n\times 1}, \tag{18b}$$

$$W = W^{\mathsf{T}}, \tag{18c}$$

$$w_{i,j} = 0, \text{ if } (i, j) \notin \mathcal{E} \text{ and } i \neq j, \tag{18d}$$

where $\rho(S)$ is the spectral radius of S, and the convergence speed decreases with $\rho(S)$. Since W is symmetric and the spectral radius of a symmetric matrix is also its spectral norm, (18a) can be cast as the minimization of $\|W - (1/n)\mathbf{1}_{n\times 1}\mathbf{1}_{n\times 1}^{\mathsf{T}}\|$, where the operator $\|\cdot\|$ is the induced matrix 2-norm. This problem is convex and can be solved globally and efficiently.

Notice that for plug-and-play capabilities, the optimization problem should be reconsidered taking into account the new addition or removal to keep overall optimality. Otherwise, at least, the elements of W associated with their neighbors should be changed accordingly to maintain the conditions in (17).

3.2 Power Compensation

The power compensation strategy we propose in this work is illustrated in Fig. 3. It relies on sharing the power-tracking error signal with the neighbor turbines, computing the average of all power-tracking errors with limited communication range, and compensating for the estimated WF power-tracking error with an additional power reference signal $u_{\mathrm{P},i}(k)$. This ensures that power tracking at the WF level is attained.

Utilizing (4) and (5) in (1), the dynamics of the power generation is

$$P_{\mathrm{g},i}(k+1) = a_{\mathrm{P}} P_{\mathrm{g},i}(k) + b_{\mathrm{P}} \hat{P}_{\mathrm{g},i}^{\mathrm{ref}}(k) + b_{\mathrm{P}} u_{\mathrm{P},i}(k) + b_{\mathrm{P}} u_{\mathrm{T},i}(k) + q_{\mathrm{P},i}(k). \tag{19}$$

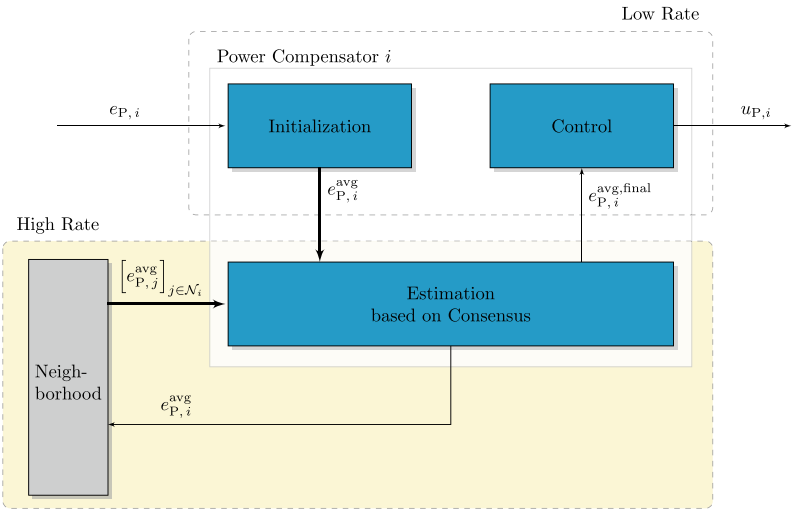


Fig. 3 Block diagram of the power compensator based on the consensus of disturbances and the number of saturated WTs

We first assume that the thrust balance control is not applied, i.e., $u_{\mathrm{T},i}(k) = 0\ \forall i$, for the application of only the power compensation. For computing the feedback control signal $u_{\mathrm{P},i}(k)$, we utilize the average power error across the entire farm obtained from the average consensus to estimate the WF power error. Our strategy is divided into Estimation and Control.

Estimation of the Average Power Tracking Error

The first step in our distributed power compensation strategy is to estimate the WF power tracking error. This is accomplished by computing the average power error at each WT using the average consensus algorithm, as discussed in Sect. 3.1. The algorithm leverages the current power error information at each WT and disseminates it by engaging in high-frequency communication with neighboring WTs.

If Assumption 2 holds, and provided that h is sufficiently large, the average consensus value is obtained in the subsequent low-rate time step. Theoretically [41, 48], we have

$$\lim_{h\to\infty} W^h e_{\mathrm{P}}(k) = \mathrm{W}_{\mathrm{avg}} e_{\mathrm{P}}(k) = e_{\mathrm{P}}^{\mathrm{avg,\ final}}(k|k+1), \tag{20}$$

where e_{P} is the vector containing all power tracking errors of each WT, W is the average consensus weight matrix, which is structured to respect the communication topology. Reiterating, $\mathrm{W}_{\mathrm{avg}}$ is the average matrix and the notation $(k|k+1)$ signifies that the average of power losses $e_{\mathrm{P}}^{\mathrm{avg,\ final}}$ from k is only obtained at $k+1$. This means that the computation of the average consensus introduces a low-rate time-step delay.

In practice, the finite value of h is determined at the design stage. It relies on the network's topology, which dictates the convergence rate, the communication speed (limiting h), and the specified tolerance level for achieving average consensus. Since W satisfies the conditions in (17), h does not affect the system stability utilizing the power compensation feedback control, but the distribution of its compensation. It moves from uniformly compensating for power errors throughout the entire farm, spreading the compensation effort, to a more localized compensation with a low finite value for h.

Control Law for Power Compensation

We propose a compensation strategy following the integral method derived for centralized controller in [17] and presented in Sect. 2.2. The integral method is demonstrated to be stable even with the presence of the additional low-rate step-time delay for the execution of the consensus algorithm. The control law uses the final estimated average power error $e_{\mathrm{P}}^{\text{avg, final}}(k-1|k)$ from the previous time step $k-1$ obtained at k, and it is defined as:

$$u_{\mathrm{P},i}(k) = u_{\mathrm{P},i}(k-1) + K_{\mathrm{P}} n e_{\mathrm{P},i}^{\text{avg, final}}(k-1|k), \tag{21}$$

where K_{P} is the integrator gain for the power compensator. In vector form, we can rewrite (21) as

$$u_{\mathrm{P}}(k) = u_{\mathrm{P}}(k-1) + \bar{K}_{\mathrm{P}} \mathrm{W}_{\mathrm{P}} e_{\mathrm{P}}(k-1), \tag{22}$$

where $\bar{K}_{\mathrm{P}}$ is the gain matrix defined as $\bar{K}_{\mathrm{P}} := \mathrm{diag}(K_{\mathrm{P}})$, and $\mathrm{W}_{\mathrm{P}} = nW^h$ a weight matrix. Notice that differing from a central control law (11), the average depends on the value of h, if $h \to \infty$ then $\mathrm{W}_{\mathrm{P}} = n\mathrm{W}_{\text{avg}}$. Importantly, the computation of the average consensus adds a sampling time delay represented by the previous power error signal e_{P} instead of the current one.

Remark 1 With the control law (21) utilizing the average consensus with a sufficiently large h, the compensation equally spreads the additional power demand, as in the centralized approach. This approach is simple and effective. Furthermore, the compensation can be expanded to take the intensity of the turbine interactions into account in (21), e.g. using a WF model-based optimization [16], or estimations of available power [15]. A weighted approach across the turbines considering the intensity of the interactions is a direct extension. However, the MCDC combines power compensation with aerodynamic load balancing, promoting a power distribution that leads to uniform degradation and prevents turbine saturation. ◁

The stability of WF with the proposed power compensation feedback control is assessed by closing the loop with the proposed average consensus algorithm and control law. Thus, we convert (19) and (22) from discrete-time description to the z-domain [49], and reorganize them using matrix algebra:

$$P_{\mathrm{g}} = (I_n z - A_{\mathrm{P}})^{-1}(B_{\mathrm{P}}\hat{P}_{\mathrm{g}}^{\mathrm{ref}} + B_{\mathrm{P}}u_{\mathrm{P}} + q_{\mathrm{P}}), \tag{23}$$

$$u_{\mathrm{P}} = (I_n z - I_n)^{-1}\bar{K}_{\mathrm{P}}\mathrm{W}_{\mathrm{P}}e_{\mathrm{P}}, \tag{24}$$

where P_{g}, u_{P}, $\hat{P}_{\mathrm{g}}^{\mathrm{ref}}$ and q_{P} represent the Z-transform of the respective vectors, calculated as $Z\,[x(k+a)] = z^a x(z)$ with $a \in \mathbb{Z}$. Then, replacing (24) into (23), utilizing the definition of the power error as $e_{\mathrm{P}} = \hat{P}_{\mathrm{g}}^{\mathrm{ref}} - P_{\mathrm{g}}$, and reorganizing it, we have the closed-loop transfer functions:

$$\frac{e_{\mathrm{P}}}{\hat{P}_{\mathrm{g}}^{\mathrm{ref}}} = (I_n z^2 + (-A_{\mathrm{P}} - I_n)z + A_{\mathrm{P}} + B_{\mathrm{P}}\bar{K}_{\mathrm{P}}\mathrm{W}_{\mathrm{P}})^{-1}(I_n z - I_n)(I_n z - A_{\mathrm{P}} - B_{\mathrm{P}}); \tag{25}$$

$$\frac{e_{\mathrm{P}}}{q_{\mathrm{P}}} = -(I_n z^2 + (-A_{\mathrm{P}} - I_n)z + A_{\mathrm{P}} + B_{\mathrm{P}}\bar{K}_{\mathrm{P}}\mathrm{W}_{\mathrm{P}})^{-1}(I_n z - I_n). \tag{26}$$

The stability of WF with the proposed power compensation feedback control is assessed through Theorem 1.

Theorem 1 *The closed loop of the MIMO system represented in (23) with the control law (24) is stable if the following linear matrix inequalities hold:*

$$B_{\mathrm{P}}\bar{K}_{\mathrm{P}}\mathrm{W}_{\mathrm{P}} > 0, \tag{27a}$$

$$A_{\mathrm{P}} + B_{\mathrm{P}}\bar{K}_{\mathrm{P}}\mathrm{W}_{\mathrm{P}} < I_n. \tag{27b}$$

Proof To prove stability, we must guarantee that the solutions to the characteristic polynomial

$$\det(I_n z^2 + (-A_{\mathrm{P}} - I_n)z + A_{\mathrm{P}} + B_{\mathrm{P}}\bar{K}_{\mathrm{P}}W_{\mathrm{P}}) = 0 \tag{28}$$

lie within the unit circle. To demonstrate this, we rely on the multivariate extension of the Jury stability criterion [50] as presented in [51]. Specifically, let us start by defining $Q(z) = Iz^2 + (-A_{\mathrm{P}} - I_n)z + A_{\mathrm{P}} + B_{\mathrm{P}}\bar{K}_{\mathrm{P}}W_{\mathrm{P}}$. Then, it follows that $\det(Q(z)) = 0$ iff $\exists x \neq 0$ such that $x^\top Q(z)x = 0$. Thus, solving (28) and verifying its solutions is equivalent to evaluating

$$\begin{aligned} x^\top Q(z)x &= x^\top(I_n z^2 + (-A_{\mathrm{P}} - I_n)z + A_{\mathrm{P}} + B_{\mathrm{P}}\bar{K}_{\mathrm{P}}W_{\mathrm{P}})x \\ &= x^\top A_2 x z^2 + x^\top A_1 x z + x^\top A_0 x \\ &= 0, \end{aligned} \tag{29}$$

where $A_2 = I_n$, $A_1 = -A_{\mathrm{P}} - I_n$, $A_0 = A_{\mathrm{P}} + B_{\mathrm{P}}\bar{K}_{\mathrm{P}}W_{\mathrm{P}}$. Note that in (29), terms $x^\top A_2 x$, $x^\top A_1 x$, $x^\top A_0 x$ are scalar. It is possible to exploit the Jury stability criterion [50], which states that having solutions of $\det(Q(z)) = 0$ restricted to the complex unit disc is equivalent to satisfying the stability constraints of the second-order polynomial (29), such that

$$\begin{cases} x^{\mathsf{T}}(A_2 + A_1 + A_0)x > 0, & \text{(30a)} \\ x^{\mathsf{T}}(A_2 - A_1 + A_0)x > 0, & \text{(30b)} \\ x^{\mathsf{T}}(A_2 - A_0)x > 0. & \text{(30c)} \end{cases}$$

In turn, given that A_2, A_1, A_0 are symmetric by construction, the conditions in (30) are equivalent to the matrix inequalities

$$\begin{cases} A_2 + A_1 + A_0 > 0, & \text{(31a)} \\ A_2 - A_1 + A_0 > 0, & \text{(31b)} \\ A_2 - A_0 > 0. & \text{(31c)} \end{cases}$$

By substituting the definition of the matrices in (31), we obtain

$$\begin{cases} B_{\mathrm{P}}\bar{K}_{\mathrm{P}}\mathrm{W}_{\mathrm{P}} > 0, & \text{(32a)} \\ 2I_n + 2A_{\mathrm{P}} + B_{\mathrm{P}}\bar{K}_{\mathrm{P}}\mathrm{W}_{\mathrm{P}} > 0, & \text{(32b)} \\ I_n - A_{\mathrm{P}} - B_{\mathrm{P}}\bar{K}_{\mathrm{P}}\mathrm{W}_{\mathrm{P}} > 0. & \text{(32c)} \end{cases}$$

Finally, (32a) is a sufficient condition for (32b), as $2I_n + 2A_{\mathrm{P}} > 0$. Indeed, this holds because $A_{\mathrm{P}} = a_{\mathrm{P}} I_n$ and $|a_{\mathrm{P}}| < 1$, conceived by the stability of the closed-loop system of the wind turbine with its local controller. This completes the proof. □

In addition to the stability conditions from (27), the disturbances q_{P} are acknowledged as bounded, as substantiated by the following assessments:

1. The contribution of the inflow turbulence or other unmodelled effects is bounded, such that $|q_{\mathrm{P},i}| < K_1$, where $K_1 \in \mathbb{R}$, governed by the convergence of the dedicated feedback controller at each WT;
2. Owing to potential saturation $q_{\mathrm{P},i} < 0$, and $q_{\mathrm{P},i} \geq -P_{\mathrm{g},i}^{\mathrm{rated}}$, as a result of the constraints imposed by the turbines and the reference signal, $P_{\mathrm{g},i} \geq 0$, $P_{\mathrm{g},i}^{\mathrm{ref}} \geq 0$, and $P_{\mathrm{g},i}^{\mathrm{ref}} \leq P_{\mathrm{g},i}^{\mathrm{rated}}$;

Therefore, based on the Bounded Input Bounded Output stability concept, the stable closed-loop system ensures that the norm of the power error remains bounded for the bounded disturbances.

3.3 *Power Distribution*

In a fully distributed WF system, aside from power compensation, the desired power references $\hat{P}_{\mathrm{g},i}^{\mathrm{ref}}(k)$ can also be addressed in a distributed manner. The information regarding the desired power reference for each turbine can be disseminated throughout the network by solving the *alignment problem* [40], also known as leader-follower consensus.

The alignment problem is accomplished by converging all the desired power references to leader turbines. The leader turbines leave their values unchanged, while all

others asymptotically agree with them according to the consensus protocol, achieving alignment. The leader-follower consensus is conducted between the WF control sampling time, adhering to the notations outlined in Sect. 3.1.

A widely employed benchmark approach is to divide the WF power reference uniformly among all WTs [15]. Thus, our proposal entails a uniform power reference distribution and assumes a single leader. The leader's power reference is determined by dividing the total WF power reference $P_{\text{WF}}^{\text{ref}}$ by the number of WTs in the WF; such that the *(re-)initialization* of the leader turbines is defined as follows

$$P_{\text{g},m}^{\text{ref, align}}(0) = P_{\text{WF}}^{\text{ref}}(k)/n, \tag{33}$$

while the *(re-)initialization* of the other turbines is

$$P_{\text{g},i}^{\text{ref, align}}(0) = \hat{P}_{\text{g},i}^{\text{ref}}(k-1), \forall i \neq m, \tag{34}$$

where $P_{\text{g},i}^{\text{ref, align}}$ is the internal state variable.

Then, in the *inner iteration* stage, the leader's power reference remains constant, being

$$P_{\text{g},m}^{\text{ref, align}}(c+1) = P_{\text{g},m}^{\text{ref, align}}(c), \forall c = 0, 1, ..., h-1. \tag{35}$$

On the other hand, the followers $i \neq m$ converge to the leader as:

$$\hat{P}_{\text{g},i}^{\text{ref, align}}(c+1) = a_{i,i}\hat{P}_{\text{g},i}^{\text{ref, align}}(c) + \sum_{j \in \mathcal{N}_i \setminus m} a_{i,j}\hat{P}_{\text{g},j}^{\text{ref, align}}(c) + b_i P_{\text{g},m}^{\text{ref, align}}(c), \tag{36}$$

$\forall c = 0, 1, ..., h-1$, where $a_{i,j} \in \mathbb{R}$, and b_i is either $\beta_i \in \mathbb{R}$ if agent i is connected to the leader, or 0 otherwise.

At the *final assignment* stage,

$$\hat{P}_{\text{g},i}^{\text{ref}}(k|k+1) = P_{\text{g},i}^{\text{ref, align}}(h), \forall i. \tag{37}$$

For a single leader, without loss of generality, we can assume that this agent is the one labeled with $m = n$. Then, the multi-agent system is said to achieve alignment between the WF control sampling time when

$$\lim_{h \to \infty} ||\hat{P}_{\text{g},i}^{\text{ref}}(k|k+1) - \hat{P}_{\text{g},n}^{\text{ref}}(k|k+1)|| = 0, \tag{38}$$

$\forall i \in \{1, 2, ..., n-1\}$. The *inner iteration* defined by (35) and (36) can be written in state form as

$$\begin{bmatrix} P_{i=1:n-1}^{\text{ref, align}}(c+1) \\ P_n^{\text{ref, align}}(c+1) \end{bmatrix} = \underbrace{\left[\begin{array}{c|c} A_{\text{lf}} & B_{\text{lf}} \\ \hline 0_{1\times n-1} & 1_{1\times 1} \end{array}\right]}_{L_{\text{lf}}} \begin{bmatrix} P_{i=1:n-1}^{\text{ref, align}}(c) \\ P_n^{\text{ref, align}}(c) \end{bmatrix}, \tag{39}$$

where $A_{\text{lf}} = [a_{i,j}]$, where $a_{i,j} = 0$ for $j \notin \mathcal{N}_i$, and $B_{\text{lf}} = [b_i]$. The design of the parameters $a_{i,j}$ and b_i is conducted by an equivalency with the alignment problem derived in [40]. It then follows

$$A_{\text{lf}} = \left(I_{n-1} + \mathcal{D}_{n-1\times n-1} + B'\right)^{-1} \left(I_{n-1} + \mathcal{A}_{n-1\times n-1}\right), \tag{40}$$

$$B_{\text{lf}} = \left(I_{n-1} + \mathcal{D}_{n-1\times n-1} + B'\right)^{-1} B', \tag{41}$$

where B' is a $n-1 \times n-1$ diagonal matrix whose ith diagonal element is 1, if i is the neighbor of the leader, and 0 otherwise; $\mathcal{D}_{n-1\times n-1}$ and $\mathcal{A}_{n-1\times n-1}$ are the degree and adjacency matrices removing the last column and row, respectively. In this way, L_{lf} in (39) is an stochastic matrix, i.e., $L_{\text{lf}}\mathbf{1}_{n\times 1} = \mathbf{1}_{n\times 1}$ and L_{lf} is square with all entries non-negative.

Utilizing this approach, the distribution of WF power reference is not made by a central workstation to each turbine, as typically observed in the general centralized scenario. Instead, the communication is distributed in exchange for a time-step delay. This time-step delay, on the other hand, can be designed to be as small as necessary, constrained by the execution of the consensus algorithm.

3.4 Thrust Balance Control

Additionally, we aim to evenly distribute the thrust forces throughout the entire farm, achieving this goal in a distributed manner. Our solution in this section also takes advantage of the average consensus and the time-scale separation from the WF and WT controllers to compute the average thrust forces. Substituting (5) into (4), and further into (2), we have

$$F_{\text{T},i}(k+1) = a_{\text{T}} F_{\text{T},i}(k) + b_{\text{T}} u_{\text{T},i}(k) + b_{\text{T}} \hat{P}^{\text{ref}}_{\text{g},i}(k) + b_{\text{T}} u_{\text{P},i}(k) + q_{\text{T},i}(k). \tag{42}$$

Initially, we assume the employment of only the thrust force balance, such that $u_{\text{P},i}(k) = 0\ \forall i$. For computing the feedback control signal $u_{\text{T},i}(k)$, we use the average thrust force across the entire farm obtained from the average consensus. Then, we estimate the thrust force errors from the average thrust force to the current values.

Estimation of the Average Thrust Force

The thrust force errors from the average thrust force to the current values are estimated for our distributed thrust force balance strategy. This is achieved by computing the average thrust force across the WF at each WT employing the average consensus algorithm from Sect. 3.1. The thrust force tracking errors $e_{\text{T},i}$ is defined as

$$e_{\text{T},i}(k) = F^{\text{avg}}_{\text{T},i}(k) - F_{\text{T},i}(k), \tag{43}$$

where $F_{\mathrm{T},i}^{\mathrm{avg}}$ is the average of thrust forces known at i-th WT and $F_{\mathrm{T},i}$ the current thrust forces.

Different from the centralized controller, $F_{\mathrm{T},i}^{\mathrm{avg}}$ is computed across the WF by the average consensus algorithm from Sect. 3.1, such that the estimation of the thrust force errors are

$$e_{\mathrm{T}}(k-1|k) = \left(W^h - I_n\right) F_{\mathrm{T}}(k-1) = -\mathrm{W}_{\mathrm{T}} F_{\mathrm{T}}(k-1), \tag{44}$$

where $\mathrm{W}_{\mathrm{T}} = -\left(W^h - I_n\right)$. When $h \to \infty$,

$$e_{\mathrm{T}}(k-1|k) = \left(\mathrm{W}_{\mathrm{avg}} - I_n\right) F_{\mathrm{T}}(k-1). \tag{45}$$

This indicates that the strategy introduces a sampling time delay besides the consensus algorithm being conducted with a finite h in practice.

Control Law for Balancing Thrust Forces

The control protocol that balances the thrust force is proposed to be pure integrators. The sampling time delay originating from the computation of the average consensus is integrated into the control law

$$u_{\mathrm{T},i}(k) = u_{\mathrm{T},i}(k-1) + K_{\mathrm{T}} e_{\mathrm{T},i}(k-1|k), \tag{46}$$

by considering a delay in the error signals (44), contrasting with the central control law in (9). Likewise, (46) can be rewritten in a vector form as:

$$\begin{aligned} u_{\mathrm{T}}(k) &= u_{\mathrm{T}}(k-1) + \bar{K}_{\mathrm{T}} e_{\mathrm{T}}(k-1|k) \\ &= u_{\mathrm{T}}(k-1) - \bar{K}_{\mathrm{T}} \mathrm{W}_{\mathrm{T}} F_{\mathrm{T}}(k-1), \end{aligned} \tag{47}$$

where $\bar{K}_{\mathrm{T}} = \mathrm{diag}(K_{\mathrm{T}})$.

Remark 2 Note that the weight matrix W_{T} is a double-stochastic matrix, based in the conditions in (17), therefore it guarantees that $\sum_i u_{\mathrm{T},i}(k) = 0\ \forall k$ by construction. Taking

$$\begin{aligned} \sum_i u_{\mathrm{T},i}(k) &= \mathbf{1}_{1\times n} u_{\mathrm{T}}(k) \\ &= \mathbf{1}_{1\times n} u_{\mathrm{T}}(0) \ + \sum_{\tau=1}^{k} \mathbf{1}_{1\times n} \bar{K}_{\mathrm{T}} e_{\mathrm{T}}(\tau - 1) \end{aligned} \tag{48}$$

and given that $u_{\mathrm{T},i}(0) = 0\ \forall i$ is established as the initial condition for the integrators, ensuring $\mathbf{1}_{1\times n} e_{\mathrm{T}}(k) = 0\ \forall k$ is a sufficient condition for $\sum_i u_{\mathrm{T},i}(k) = 0\ \forall k$. Then, by (44), it is apparent that

$$\mathbf{1}_{1\times n} e_{\mathrm{T}}(k) = -\mathbf{1}_{1\times n} \mathrm{W}_{\mathrm{T}} F_{\mathrm{T}}(k) = \mathbf{1}_{1\times n} \left(W^h - I_n\right) = 0 \tag{49}$$

where $\mathbf{1}_{1\times n} W^h = \mathbf{1}_{1\times n}$ as W^h is a double-stochastic matrix. ◁

Remark 3 When turbine saturation occurs, the balancing of thrust forces reduces the WF power generation. The saturated turbine can not increase power generation and it has a lower thrust force compared to the remaining turbines. Consequently, the saturated turbine affects the power generation of the other turbines by diminishing their power output and failing to compensate for their reduced generation with its own increased power generation. ◁

Hence, we exclude saturated turbines from the balancing of thrust forces, departing from the previous practice in the centralized control approach in [12, 17]. This prioritizes power generation and is justified by the fact that the thrust forces of saturated turbines are lower than the remaining ones.

To accomplish this, we define the consensus algorithm, such that W^h reaches the definition of the average matrix in (50) when $h \to \infty$.

$$\mathrm{W}_{\mathrm{avg}} = [\mathrm{w}_{\mathrm{avg},i,j}] = \begin{cases} 1, & \text{if } i = j \text{ is saturated,} \\ 0, & \text{if } i \neq j \text{ and } i \text{ or } j \text{ is saturated,} \\ \frac{1}{n-n_{\mathrm{S}}}, & \text{otherwise,} \end{cases} \tag{50}$$

where n_{S} is the number of saturated turbines. The double-stochasticity property persists and the thrust force error of the saturated turbines is zero, granting an anti-windup property for the integrators. An example of the weighted matrix of a 3-turbine farm with saturation in the second turbine is

$$\mathrm{W}_{\mathrm{avg}} = \begin{bmatrix} \frac{1}{2} & 0 & \frac{1}{2} \\ 0 & 1 & 0 \\ \frac{1}{2} & 0 & \frac{1}{2} \end{bmatrix}.$$

In vector form, (42) becomes

$$F_{\mathrm{T}}(k+1) = A_{\mathrm{T}} F_{\mathrm{T}}(k) + B_{\mathrm{T}} u_{\mathrm{T}}(k) + B_{\mathrm{T}} \hat{P}_{\mathrm{g}}^{\mathrm{ref}}(k) + q_{\mathrm{T}}(k), \tag{51}$$

where $A_{\mathrm{T}} = \mathrm{diag}(a_{\mathrm{T}})$ and $B_{\mathrm{T}} = \mathrm{diag}(b_{\mathrm{T}})$.

In the z-domain, (51) and (47) become

$$F_{\mathrm{T}} = (I_n z - A_{\mathrm{T}})^{-1} [B_{\mathrm{T}} u_{\mathrm{T}} + B_{\mathrm{T}} \hat{P}_{\mathrm{g}}^{\mathrm{ref}} + q_{\mathrm{T}}], \tag{52}$$

$$u_{\mathrm{T}} = (I_n z - I_n)^{-1} \bar{K}_{\mathrm{T}} e_{\mathrm{T}}, \tag{53}$$

where $F_{\mathrm{T}}, u_{\mathrm{T}}, \hat{P}_{\mathrm{g}}^{\mathrm{ref}}$ and q_{T} represent the Z-transform of their respective vectors. Then, replacing (53) into (52), and utilizing (44), we have the close-loop transfer functions

$$\frac{e_{\mathrm{T}}}{\hat{P}_{\mathrm{g}}^{\mathrm{ref}}} = -(I_n z^2 - (A_{\mathrm{T}} + I_n)z + A_{\mathrm{T}} + \mathrm{W}_{\mathrm{T}} B_{\mathrm{T}} \bar{K}_{\mathrm{T}})^{-1} B_{\mathrm{T}} (I_n z - I_n) \mathrm{W}_{\mathrm{T}}, \tag{54}$$

$$\frac{e_{\mathrm{T}}}{q_{\mathrm{T}}} = -(I_n z^2 - (A_{\mathrm{T}} + I_n)z + A_{\mathrm{T}} + \mathrm{W}_{\mathrm{T}} B_{\mathrm{T}} \bar{K}_{\mathrm{T}})^{-1} (I_n z - I_n) \mathrm{W}_{\mathrm{T}}. \tag{55}$$

Thus, the stability of WF with the thrust balance control is assessed through Theorem 2.

Theorem 2 *The stability of the closed loop for the MIMO system described in (52), governed by the control law (53) is guaranteed when the following linear matrix inequalities hold:*

$$W_T B_T \bar{K}_T > 0, \tag{56a}$$

$$A_T + W_T B_T \bar{K}_T < I_n. \tag{56b}$$

Proof To prove stability, we must guarantee that the solutions to the characteristic polynomial

$$\det(I_n z^2 - (A_{\mathrm{T}} + I_n)z + A_{\mathrm{T}} + \mathrm{W}_{\mathrm{T}} B_{\mathrm{T}} \bar{K}_{\mathrm{T}}) = 0 \tag{57}$$

lie within the unit circle. Similar to the proof of Theorem 1, it follows that $\det(Q(z)) = 0$ iff $\exists x \neq 0$ such that $x^{\top} Q(z) x = 0$. Thus, evaluating

$$x^T (I_n z^2 - (A_{\mathrm{T}} + I_n)z + A_{\mathrm{T}} + \mathrm{W}_{\mathrm{T}} B_{\mathrm{T}} \bar{K}_{\mathrm{T}}) x = 0$$

by utilizing the Jury stability criterion, we have

$$\begin{cases} \mathrm{W}_{\mathrm{T}} B_{\mathrm{T}} \bar{K}_{\mathrm{T}} > 0, & \text{(58a)} \\ 2I_n + 2A_{\mathrm{T}} + \mathrm{W}_{\mathrm{T}} B_{\mathrm{T}} \bar{K}_{\mathrm{T}} > 0, & \text{(58b)} \\ I_n - A_{\mathrm{T}} - \mathrm{W}_{\mathrm{T}} B_{\mathrm{T}} \bar{K}_{\mathrm{T}} > 0. & \text{(58c)} \end{cases}$$

Since the power tracking controllers at each individual WT are stable, $-1 < a_{\mathrm{T},i} < 1$ for all i. Consequently, $2I_n + 2A_{\mathrm{T}} > 0$. Then, as $\mathrm{W}_{\mathrm{T}} \geq 0$ by definition, (58b) holds for all $\bar{K}_{\mathrm{T}}$ such that $\mathrm{W}_{\mathrm{T}} B_{\mathrm{T}} \bar{K}_{\mathrm{T}} > 0$. Therefore, the control designer must select $\bar{K}_{\mathrm{T}}$ that satisfies (58a) and (58c). □

Finally, an assessment of the stability of WF with both feedback loops for power compensation and thrust force balancing is conducted to account for their reciprocal impact when they are implemented simultaneously in the MCDC approach. Previously, the stability was assessed for the implementation of the feedback loop independently. However, upon closing both feedback loops, due to the consensus algorithm, the dynamics of one loop affects the other and vice-versa. Therefore, the stability of the system with both the power compensator and the thrust force balance is verified utilizing the following theorem:

Theorem 3 *The closed-loop stability, utilizing both feedback control laws (24) and (53) simultaneously, is ensured when the following linear matrix inequalities are satisfied:*

$$A_0 - A_3 < 0, \tag{59a}$$
$$A_0 + A_1 + A_2 + A_3 > 0, \tag{59b}$$
$$A_0 - A_1 + A_2 - A_3 < 0, \tag{59c}$$

and

$$\begin{vmatrix} A_0 & A_3 \\ A_3 & A_0 \end{vmatrix} > \begin{vmatrix} A_0 & A_1 \\ A_3 & A_2 \end{vmatrix}, \tag{60}$$

where $A_3 = I_n$, $A_2 = -(I_n + A_P + A_T)$, $A_1 = A_P A_T + A_P + A_T + B_P \bar{K}_P W_P + W_T B_T \bar{K}_T$, $A_0 = -A_P A_T - A_T B_P \bar{K}_P W_P + A_P W_T B_T \bar{K}_T$, *and* $|.|$ *is the determinant operation.*

Proof Taking the vector form of the power reference from (4), and utilizing (5) with the control laws (24) and (53), we have

$$P_{\mathrm{g}}^{\mathrm{ref}} = \hat{P}_{\mathrm{g}}^{\mathrm{ref}} + u_{\mathrm{P}} + u_{\mathrm{T}} \tag{61a}$$
$$= \hat{P}_{\mathrm{g}}^{\mathrm{ref}} + C_{\mathrm{P}} \mathrm{W}_{\mathrm{P}} e_{\mathrm{P}} + C_{\mathrm{T}} e_{\mathrm{T}} \tag{61b}$$
$$= \hat{P}_{\mathrm{g}}^{\mathrm{ref}} + C_{\mathrm{P}} \mathrm{W}_{\mathrm{P}} (\hat{P}_{\mathrm{g}}^{\mathrm{ref}} - P_{\mathrm{g}}) - C_{\mathrm{T}} \mathrm{W}_{\mathrm{T}} F_{\mathrm{T}} \tag{61c}$$
$$= \hat{P}_{\mathrm{g}}^{\mathrm{ref}} + C_{\mathrm{P}} \mathrm{W}_{\mathrm{P}} [\hat{P}_{\mathrm{g}}^{\mathrm{ref}} - (G_{\mathrm{P}} P_{\mathrm{g}}^{\mathrm{ref}} + q_{\mathrm{P}})] - C_{\mathrm{T}} \mathrm{W}_{\mathrm{T}} (G_{\mathrm{T}} P_{\mathrm{g}}^{\mathrm{ref}} + q_{\mathrm{T}}) \tag{61d}$$
$$= (I_n + C_{\mathrm{P}} \mathrm{W}_{\mathrm{P}}) \hat{P}_{\mathrm{g}}^{\mathrm{ref}} - C_{\mathrm{P}} \mathrm{W}_{\mathrm{P}} G_{\mathrm{P}} P_{\mathrm{g}}^{\mathrm{ref}} - C_{\mathrm{T}} \mathrm{W}_{\mathrm{T}} G_{\mathrm{T}} P_{\mathrm{g}}^{\mathrm{ref}} - C_{\mathrm{P}} \mathrm{W}_{\mathrm{P}} q_{\mathrm{P}} - C_{\mathrm{T}} \mathrm{W}_{\mathrm{T}} q_{\mathrm{T}} \tag{61e}$$
$$= (I_n + C_{\mathrm{P}} \mathrm{W}_{\mathrm{P}} G_{\mathrm{P}} + C_{\mathrm{T}} \mathrm{W}_{\mathrm{T}} G_{\mathrm{T}})^{-1} [(I_n + C_{\mathrm{P}} \mathrm{W}_{\mathrm{P}}) \hat{P}_{\mathrm{g}}^{\mathrm{ref}} - C_{\mathrm{P}} \mathrm{W}_{\mathrm{P}} q_{\mathrm{P}} - C_{\mathrm{T}} \mathrm{W}_{\mathrm{T}} q_{\mathrm{T}}], \tag{61f}$$

where $C_{\mathrm{P}} = (I_n z - I_n)^{-1} \bar{K}_{\mathrm{P}}$, $C_{\mathrm{T}} = (I_n z - I_n)^{-1} \bar{K}_{\mathrm{T}}$, $G_{\mathrm{P}} = (I_n z - A_{\mathrm{P}})^{-1} B_{\mathrm{P}}$, and $G_{\mathrm{T}} = (I_n z - A_{\mathrm{T}})^{-1} B_{\mathrm{T}}$, are the open-loop power compensator, thrust force balancer, turbines' power and thrust force transfer functions, respectively. The feedback system is illustrated in the block diagram in Fig. 4. The input disturbance d_{i} is taken as the feedforward term, which is the reference power $\hat{P}_{\mathrm{g}}^{\mathrm{ref}}$. Substituting the transfer functions accordingly and utilizing algebra manipulations

$$\begin{aligned}(I_n + C_{\mathrm{P}} \mathrm{W}_{\mathrm{P}} G_{\mathrm{P}} + C_{\mathrm{T}} \mathrm{W}_{\mathrm{T}} G_{\mathrm{T}})^{-1} = {} & [(I_n z - A_{\mathrm{P}})(I_n z - A_{\mathrm{T}})(I_n z - I_n) \\ & + (I_n z - A_{\mathrm{T}}) \bar{K}_{\mathrm{P}} \mathrm{W}_{\mathrm{P}} B_{\mathrm{P}} + (I_n z - A_{\mathrm{P}}) \bar{K}_{\mathrm{T}} \mathrm{W}_{\mathrm{T}} B_{\mathrm{T}}]^{-1} \\ & [(I_n z - A_{\mathrm{P}})(I_n z - A_{\mathrm{T}})(I_n z - I_n)].\end{aligned} \tag{62}$$

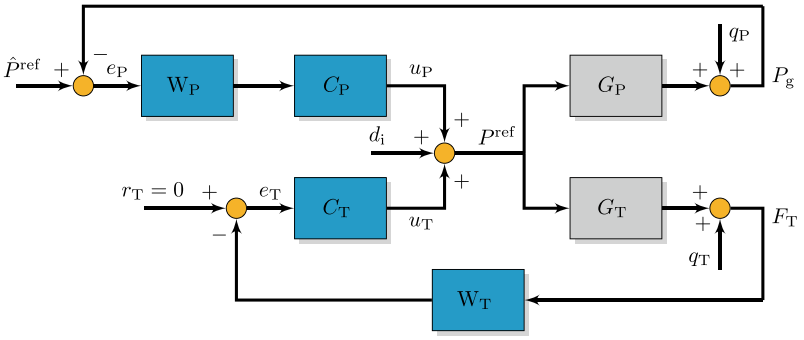


Fig. 4 Block diagram of the closed-loop system representing the communication by the definition of W_{P} and W_{T}

The closed-loop power and thrust dynamic behavior due to changes in the reference power, power discrepancy, and thrust force discrepancy are

$$\begin{aligned} P_{\text{g}} &= G_{\text{P}} P_{\text{g}}^{\text{ref}} \\ &= [(I_n z - A_{\text{P}})(I_n z - A_{\text{T}})(I_n z - I_n) + (I_n z - A_{\text{T}})\bar{K}_{\text{P}}\text{W}_{\text{P}}B_{\text{P}} + (I_n z - A_{\text{P}})\bar{K}_{\text{T}}\text{W}_{\text{T}}B_{\text{T}}]^{-1} \\ &\quad [B_{\text{P}}(I_n z - A_{\text{T}})(I_n z - I_n + \bar{K}_{\text{P}}\text{W}_{\text{P}})\hat{P}_{\text{g}}^{\text{ref}} - B_{\text{P}}\bar{K}_{\text{P}}\text{W}_{\text{P}}q_{\text{P}} - B_{\text{P}}\bar{K}_{\text{T}}\text{W}_{\text{T}}q_{\text{T}}], \end{aligned} \tag{63}$$

$$\begin{aligned} F_{\text{T}} &= G_{\text{T}} P_{\text{g}}^{\text{ref}} \\ &= [(I_n z - A_{\text{P}})(I_n z - A_{\text{T}})(I_n z - I_n) + (I_n z - A_{\text{T}})\bar{K}_{\text{P}}\text{W}_{\text{P}}B_{\text{P}} + (I_n z - A_{\text{P}})\bar{K}_{\text{T}}\text{W}_{\text{T}}B_{\text{T}}]^{-1} \\ &\quad [B_{\text{T}}(I_n z - A_{\text{P}})(I_n z - I_n + \bar{K}_{\text{P}}\text{W}_{\text{P}})\hat{P}_{\text{g}}^{\text{ref}} - B_{\text{T}}\bar{K}_{\text{P}}\text{W}_{\text{P}}q_{\text{P}} - B_{\text{T}}\bar{K}_{\text{T}}\text{W}_{\text{T}}q_{\text{T}}]. \end{aligned} \tag{64}$$

To ensure stability, we must guarantee that the solutions to the characteristic polynomial

$$\det\left((I_n z - A_{\text{P}})(I_n z - A_{\text{T}})(I_n z - I_n) + (I_n z - A_{\text{T}})\bar{K}_{\text{P}}\text{W}_{\text{P}}B_{\text{P}} + (I_n z - A_{\text{P}})\bar{K}_{\text{T}}\text{W}_{\text{T}}B_{\text{T}}\right) = 0 \tag{65}$$

lie within the unit circle. This condition is equivalent to evaluate

$$\begin{aligned} &x^{\top}\left((I_n z - A_{\text{P}})(I_n z - A_{\text{T}})(I_n z - I_n) + (I_n z - A_{\text{T}})\bar{K}_{\text{P}}\text{W}_{\text{P}}B_{\text{P}} + (I_n z - A_{\text{P}})\bar{K}_{\text{T}}\text{W}_{\text{T}}B_{\text{T}}\right)x = \\ &x^{\top}\Big(Iz^3 - (I_n + A_{\text{P}} + A_{\text{T}})z^2 + [A_{\text{P}}A_{\text{T}} + A_{\text{P}} + A_{\text{T}} + \bar{K}_{\text{P}}\text{W}_{\text{P}}B_{\text{P}} + \bar{K}_{\text{T}}\text{W}_{\text{T}}B_{\text{T}}]z - A_{\text{P}}A_{\text{T}} - \\ &\qquad A_{\text{T}}\bar{K}_{\text{P}}\text{W}_{\text{P}}B_{\text{P}} - A_{\text{P}}\bar{K}_{\text{T}}\text{W}_{\text{T}}B_{\text{T}}\Big)x = 0 \end{aligned} \tag{66}$$

where x is a non-zero vector. Utilizing the Jury stability criterion [50] for a third-order polynomial, the matrix conditions in (59) and (60) can be derived.

Moreover, evaluating internal stability extends beyond assessing the transfer functions derived in (63) and (64). Figure 5 depicts the MIMO closed-loop system in a

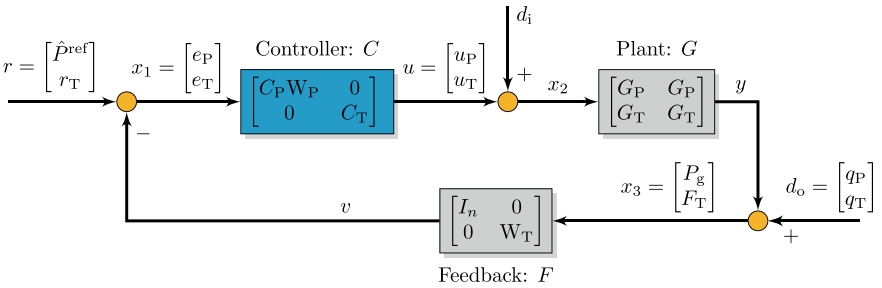


Fig. 5 Block diagram of the closed-loop system representing the communication by the definition of W_{P} and W_{T} in basic feedback loop [52]

standard feedback configuration. Following the approach in [52], the internal transfer functions are obtained by

$$\begin{bmatrix} x_1 \\ x_2 \\ x_3 \end{bmatrix} = (I_{2n} + GCF)^{-1} \begin{bmatrix} I_{2n} & -GF & -F \\ C & I_{2n} & -CF \\ GC & G & I_{2n} \end{bmatrix} \begin{bmatrix} r \\ d_{\text{i}} \\ d_{\text{o}} \end{bmatrix}, \tag{67}$$

where $G = [G_{\text{P}}\ G_{\text{P}};\ G_{\text{T}}\ G_{\text{T}}]$, $C = [C_{\text{P}}\text{W}_{\text{P}}\ 0_n;\ 0_n\ C_{\text{T}}]$, $F = [I_n\ 0_n;\ 0_n\ \text{W}_{\text{T}}]$. On a positive note, all the internal closed-loop transfer functions retain the characteristic polynomial in (65) and are well-defined and proper. Consequently, the matrix conditions in (59) and (60) ensure internal stability. □

The implication of Theorems 1 and 2 on Theorem 3 can be verified by multiplying the characteristic matrix polynomials (28) and (57).

$$\begin{aligned} \det\left((I_n z - I_n)(I_n z - A_{\text{P}}) + B_{\text{P}}\bar{K}_{\text{P}}\text{W}_{\text{P}}\right).\ \det\left((I_n z - I_n)(I_n z - A_{\text{T}}) + B_{\text{T}}\bar{K}_{\text{T}}\text{W}_{\text{T}}\right) = \\ \det\left((I_n z - I_n)\left[(I_n z - I_n)(I_n z - A_{\text{P}})(I_n z - A_{\text{T}}) + (I_n z - A_{\text{P}})B_{\text{T}}\bar{K}_{\text{T}}\text{W}_{\text{T}}\right.\right. \\ \left.\left. + (I_n z - A_{\text{T}})B_{\text{P}}\bar{K}_{\text{P}}\text{W}_{\text{P}}\right] + B_{\text{P}}\bar{K}_{\text{P}}\text{W}_{\text{P}}B_{\text{T}}\bar{K}_{\text{T}}\text{W}_{\text{T}}\right) = 0 \end{aligned} \tag{68}$$

When the consensus is achieved, i.e., $h \to \infty$, $\text{W}_{\text{P}} = n\text{W}_{\text{avg}}$ and $\text{W}_{\text{T}} = -\left(\text{W}_{\text{avg}} - I_n\right)$, $\text{W}_{\text{P}}\text{W}_{\text{T}} = 0$, therefore $B_{\text{P}}\bar{K}_{\text{P}}\text{W}_{\text{P}}B_{\text{T}}\bar{K}_{\text{T}}\text{W}_{\text{T}} = 0$.

Remark 4 The resulting product of the characteristic polynomials in (68) yields the characteristic polynomial (65) with additional roots at one when consensus is achieved. Consequently, Theorems 1 and 2 are sufficient for Theorem 3. This also holds for the centralized controller, where $\text{W}_{\text{P}}\text{W}_{\text{T}} = 0$. However, in practice, we operate with a finite number of h, such that $\text{W}_{\text{P}}\text{W}_{\text{T}} \neq 0$, then Theorem 3 becomes at hand.

4 Numerical Results

The proposed MCDC control algorithm is evaluated in the high-fidelity large-eddy simulator, SOWFA [53]. The WF layout is based on the TotalControl reference wind power plant [54], for which the studied atmospheric scenarios and power demand are defined in [17]. The set of neighbors $\mathcal{N}_i$ is established according to the communication range depicted in Fig. 6. We consider a low wake interaction scenario (Scenario 1) and a medium wake interaction scenario (Scenario 2), which differ in the prevailing wind direction given the adopted WF layout. The simulations were configured with a 10 Hz sampling rate applied to both the WT and WF controllers. The wake interactions in these scenarios are illustrated in Figs. 7 and 8, respectively.

For comparison, we also implemented the distributed averaging-based integral (DAI) controller adapted from [42–44]. Different from our approach that allows average consensus, this controller obtains current information from the local neighborhood and concurrently computes and applies the control action.

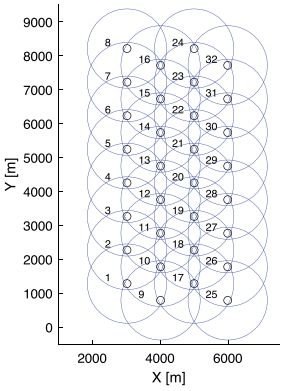


Fig. 6 Illustration of the communication range spanning $5\sqrt{2}$ of the turbine diameter. Within each blue circle, centered on the turbine location, communication is established with the enclosed turbines

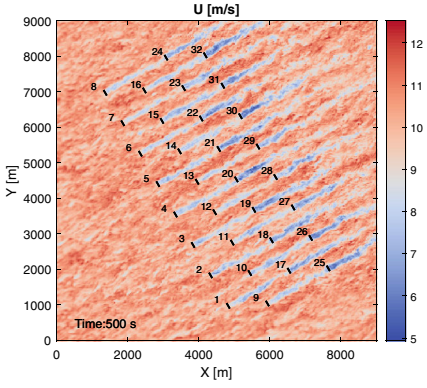


Fig. 7 The reference wind power plant in Scenario 1. Horizontal slice of the wind flow from SOWFA

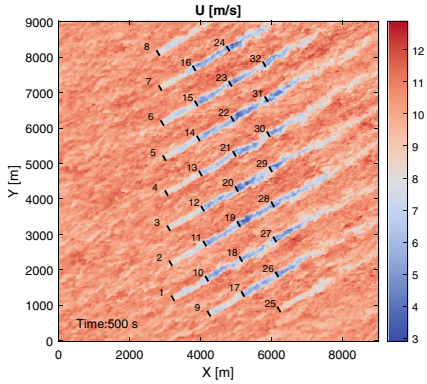


Fig. 8 The reference wind power plant in Scenario 2. Horizontal slice of the wind flow from SOWFA

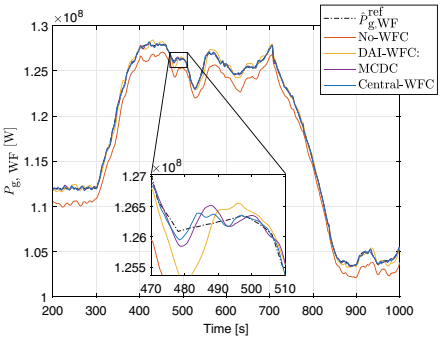


Fig. 9 Wind farm active power generation in Scenario 1

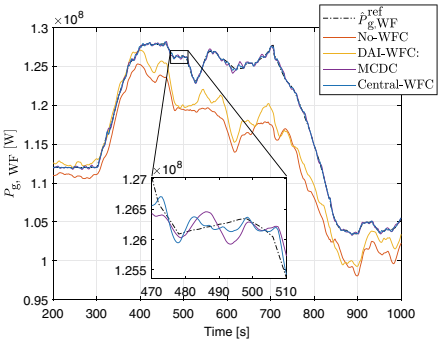


Fig. 10 Wind farm active power generation in Scenario 2

We start by presenting the comparisons of the WF's active power generation under the influence of different controllers, specifically in Scenario 1 and Scenario 2. For a visual representation, please refer to Figs. 9 and 10. A quantitative assessment of the WF's active power tracking was conducted. This evaluation is based on the root mean square error (RMSE) between the desired power reference and the actual power generation, as well as its peak error (PE). These key performance indicators are conveniently summarized in Table 1. It is important to note that the performance

Table 1 Performance of WF controllers

Scenario	Controller	RMSE of power [MW]	PE of power [MW]	Mean of thrust variance [GN^2]	Peak of thrust variance [GN^2]
1	No-WFC	1.2950	2.6982	2.3297	4.1050
	DAI-WFC	0.3412	1.1150	1.4165	2.6144
	MCDC	0.1258	0.5536	0.1883	0.3881
	Central-WFC	0.1142	0.4612	0.2723	0.6272
2	No-WFC	6.0417	10.7650	8.0316	10.9100
	DAI-WFC	4.9737	9.4981	5.0376	7.7943
	MCDC	0.2268	0.9006	0.6447	2.2425
	Central-WFC	0.1422	0.5021	0.6195	2.0546

indicators in Table 1 were calculated from the 300-second mark onward. This choice was made to ensure the removal of any transient behavior during the initiation and to allow ample time for wakes to propagate through the WF.

Shifting our focus to the structural loads, we provide a visual depiction of the thrust balancer's performance for each of the control approaches in Fig. 11. Furthermore, as outlined in Table 1, the quantitative evaluation of the thrust balancers is also presented in terms of the mean and peak of the thrust force variance across the turbines.

In scenarios characterized by high wake effects, the utilization of feedback WF controllers notably improves the accuracy of active power tracking, outperform-

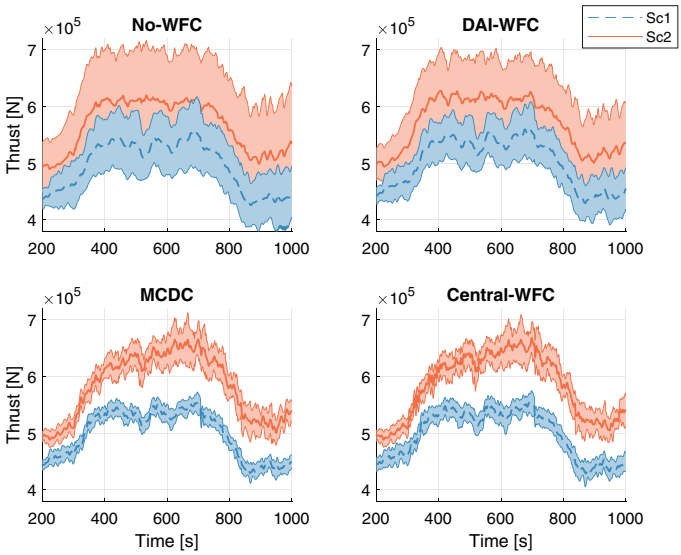


Fig. 11 Mean and standard deviation of the thrust forces in both scenarios

ing simulations where such controllers are not engaged (No-WFC). Specifically, the study case demonstrated a notable reduction of up to 97.6% and 95.3% in the RMSE and PE of the power, respectively. This significant improvement is primarily attributed to the mitigating effect on turbine saturation by the WFC. Moreover, employing WF controllers designed to balance thrust forces leads to a substantial reduction in the thrust force variations across WTs in the farm, achieving reductions of up to 92.3% and 81.2% in the mean and peak, respectively, of the thrust force variance across WTs over the duration of the simulation.

Transitioning from centralized controller (Central-WFC) to distributed control (DAI-WFC) in Scenario 2, a significant decrease in performance is evident. The Central-WFC results in a reduction of 97.14% in the RMSE of power and 87.70% in the mean of thrust force variance compared with the DAI-WFC. This is an expected outcome as the DAI-WFC lacks complete information about the entire farm, highlighted by Scenario 2 with the occurrence of turbine saturation, which hampers its ability to effectively compensate for power losses and balance thrust forces.

Our main results are centered around the effectiveness of the proposed MCDC. Despite the added delay from the average consensus computation, the MCDC still showcases comparable performance when compared to the Central-WFC. In Scenario 2, the MCDC achieves a 96.25% reduction in the RMSE of power compared with the No-WFC, comparable to the 97.6% reduction by the Central-WFC compared with the No-WFC. Similarly, the MCDC achieves a 91.97% reduction in the mean of the thrust force variance, compared to the 92.3% reduction observed with the Central-WFC. Interestingly, in Scenario 1, the MCDC overperforms the Central-WFC in terms of the thrust force balancing. This is attributed to the performance of the power compensator, which in the MCDC, due to the time-step delay, it becomes less accurate than the Central-WFC yet with lower variation. This translates to a reduction in oscillations in the aerodynamic loads observed in Scenario 1.

The MCDC relies on more frequent communication with neighboring WTs in comparison to the DAI-WFC and alternative approaches found in the existing literature. To reach average consensus, we conservatively set the number of steps at $h = 400$, a significantly large value for the considered communication network, acknowledging that the WF control's sampling time does not necessitate the same level of swiftness as the WT control. Further research will investigate strategies to reduce the number of communication steps and explore the re-initiation for fast average consensus. This will ultimately result in a decrease in the communication requirements.

5 Exploring Energy System Integration: A Discussion

The discussion about our proposed approach within the energy systems integration framework and multi-energy systems concept is presented in this section.

- **Fit into Multi-Energy Systems (MES).** Our distributed control approach for wind farms aligns well with the evolving landscape of MES by addressing power system stability challenges stemming from wind variability. By enhancing active power regulation, our approach increases the reliability of wind energy generation, a key component within MES. Advantages include enhanced modularity and sparsity, which contribute to cost-efficient energy generation, requiring a substantially less resource-intensive communication network, scalability, and grid stability. However, drawbacks such as communication issues arise in large-scale farms.
- **Integration into Energy Systems Integration (ESI) Scheme.** Our proposed approach facilitates the coupling into an ESI scheme by harnessing wind energy as a flexible energy source, thereby diverging from conventional wind energy maximization strategies. Through the implementation of our approach, we elevate the power generation capability, addressing wind variability, and thus mitigating grid stability issues.
- **Consideration of ESI in Research.** Our research focused on developing a smart solution consisting of a fully distributed control framework that regulates active power generation, disseminates power references efficiently, and achieves load balancing in wind farms. Still, to shape the future MES, comprehensive research into an entire ESI scheme is essential. This scheme must encompass alternative energy sources, storage systems, and users, ensuring sustainable and reliable operation beyond individual performances. Achieving this necessitates the concerted effort and collaboration of a multidisciplinary team working closely together.
- **Benefits within ESI Framework.** The benefits of our approach within an ESI framework include increased renewable energy integration, improved grid stability, and enhanced operational efficiency. By decentralizing control and leveraging distributed communication, our approach offers cost-effective and scalable solutions for managing wind energy resources.
- **Resources Needed for ESI Implementation.** Implementation of our solution demands fewer resources compared to a centralized control scheme, as it leverages existing turbine hardware. They include a low-range communication system to exchange information with nearby turbines and the implementation of the WF control algorithms locally in the turbine hardware.
- **Measurement of ESI Implementation Success.** The success of our approach within the MES can be measured by evaluating metrics such as on-demand power generation performance, resource utilization efficiency, and cost-effectiveness. Additionally, the reduction of aerodynamic load variability and uniform degradation of WTs are key indicators of successful implementation.
- **Metrics for Evaluating Solution Effectiveness.** Metrics for evaluating the effectiveness of our solution include power generation performance, grid stability indices, alignment of power references, and load balancing across the WF. These metrics provide insights into the performance and reliability of our solution over time.
- **Monitoring the Resultant ESI Solution.** The resultant ESI solution should be monitored over time through continuous performance monitoring. Inspections of system components, real-time monitoring of power generation and consumption,

and assessments of grid stability should be conducted to ensure the effectiveness and reliability of the solution.

6 Conclusions

As wind parks transition towards large-scale systems, the prominent future trajectory for WF control is toward decentralization. This transformation introduces numerous challenges in effectively controlling them cooperatively. In this study, we assessed distributed control strategies aimed at enhancing *modularity* and *sparsity*, while still reaching a reliable operation. These strategies, though the offering of active power tracking capability from the turbine controllers, enable the provision of ancillary services to the grid while central communication is avoided.

The main contribution of this research is the development of the MCDC, a fully distributed approach for power compensation, power distribution, and aerodynamic load balance. The findings showcase enormous potential, as the proposed MCDC enables the attainment of control performance equivalent to the centralized controller. While the high-rate communication required for average consensus may raise concerns, it is important to note that communication is limited to the neighboring WTs. This compensates for the communication overhead and allows a modular control framework. Consequently, significant cost reductions are anticipated, as the achieved *modularity* facilitates implementation/installation and industrialization of WF controllers. This paves the way for mass-producing the WF control system embedded in each turbine. The absence of a supervisory or central control system operating point further contributes to cost reduction. Additionally, as a result of the thrust balance achieved by the MCDC, there would be a reduction in costs associated with the prevention of sporadic maintenance events by evenly spreading the aerodynamic load across the turbines.

However, there are important open issues that require further investigation and resolution. One such extension of this work involves eliminating the idealized communication assumptions, such as imposing communication rate limitations, where consensus might not sufficiently converge within the sampling time of the WF control, and incorporating sampled schemes in the presence of delays [41, 55].

In conclusion, the shift towards distributed control strategies in wind farm operations represents a significant advancement in the field, promising applicability, and cost-effectiveness. The development of the MCDC presented in this study demonstrates the feasibility and effectiveness of distributed approaches in addressing the challenges of large-scale wind park management. With modular control frameworks and leveraging communication between neighboring turbines, the MCDC not only achieves comparable performance to centralized control systems but also offers potential cost savings and operational benefits.

Acknowledgements This research was supported by the European Union Horizon 2020 program through the WATEREYE project (grant no. 851207). We thank Alex Gallo and Twan Keizer, our colleagues at TU Delft, for their insightful discussions and contributions to this work.

References

1. EirGrid. Eirgrid grid code version 10.0, 2021. https://www.eirgridgroup.com/customer-and-industry/general-customer-information/grid-code-info/. Accessed: 2022-08-17
2. ENTSO-E. Entso-e network code for requirements for grid connection applicable to all generators, 2016. https://www.entsoe.eu/network_codes/. Accessed: 2022-08-17
3. ENTSO-E Technical Group HPOPEIPS. High Penetration of Power Electronic Interfaced Power Sources and the Potential Contribution of Grid Forming Converters, 2019. https://www.entsoe.eu/publications/system-operations-reports/. Accessed: 2023-04-18
4. National Grid Electricity System Operator Limited. The grid code, 2021. URL https://www.nationalgrideso.com/industry-information/codes/grid-code-gc/grid-code-documents. Issue 6, Revision 16. Accessed: 2023-04-18
5. Aho J, Fleming P, Pao LY (2016) Active power control of wind turbines for ancillary services: A comparison of pitch and torque control methodologies. In: American control conference (ACC), pp 1407–1412. https://doi.org/10.1109/ACC.2016.7525114
6. Kim K, Kim H, Kim C, Paek I, Bottasso C, Campagnolo F (2018) Design and validation of demanded power point tracking control algorithm of wind turbine. Int. J. of Precision Engineering and Manufacturing-Green Technology 5:387–400. https://doi.org/10.1007/s40684-018-0041-6
7. Lio WH, Mirzaei M, Larsen GC (2018) On wind turbine down-regulation control strategies and rotor speed set-point. J Phys Conf Ser 1037:032040. https://doi.org/10.1088/1742-6596/1037/3/032040
8. Meyers J, Bottasso C, Dykes K, Fleming P, Gebraad P, Giebel G, Göçmen T, van Wingerden J-W (2022) Wind farm flow control: prospects and challenges. Wind Energy Sci 7(6):2271–2306. https://doi.org/10.5194/wes-7-2271-2022. https://wes.copernicus.org/articles/7/2271/2022/
9. Díaz-González F, Hau M, Sumper A, Gomis-Bellmunt O (2014) Participation of wind power plants in system frequency control: Review of grid code requirements and control methods. Renew Sustain Energy Rev 34:551–564. ISSN 13640321. https://doi.org/10.1016/j.rser.2014.03.040
10. Ela E, Gevorgian V, Fleming PA, Zhang YC, Singh M, Muljadi E, Scholbrook A, Aho J, Buckspan A, Pao LY, Singhvi V, Tuohy A, Pourbeik P, Brooks D, Bhatt N (2014) Active power controls from wind power : bridging the gaps. Technical report, National Renewable Energy Laboratory (NREL)
11. Vali M, Petrović V, Steinfeld G, Pao LY, Kühn M (2019) An active power control approach for wake-induced load alleviation in a fully developed wind farm boundary layer. Wind Energy Science 4(1):139–161. https://doi.org/10.5194/wes-4-139-2019
12. Jean Gonzalez Silva, Bart Doekemeijer, Riccardo Ferrari, and Jan-Willem van Wingerden. Active power control of waked wind farms: Compensation of turbine saturation and thrust force balance. In *2021 European Control Conference (ECC)*, pages 1223–1228, 2021. https://doi.org/10.23919/ECC54610.2021.9655154
13. Poul Sørensen, Anca D Hansen, Florin Iov, Frede Blaabjerg, and Martin H Donovan. Wind farm models and control strategies. Technical Report 1464(EN), Denmark. Forskningscenter Risoe., 2005
14. Jacob Aho, Andrew Buckspan, Jason Laks, Paul Fleming, Yunho Jeong, Fiona Dunne, Matthew Churchfield, Lucy Pao, and Kathryn Johnson. A tutorial of wind turbine control for supporting grid frequency through active power control. In *2012 American Control Conference (ACC)*, pages 3120–3131, 2012. https://doi.org/10.1109/ACC.2012.6315180

15. Knudsen Torben, Bak Thomas, Svenstrup Mikael (2015) Survey of wind farm controlâ??power and fatigue optimization. Wind Energy 18(8):1333–1351. https://doi.org/10.1002/we.1760
16. Jennifer Annoni, Pieter M. O. Gebraad, Andrew K. Scholbrock, Paul A. Fleming, and Jan-Willem van Wingerden. Analysis of axial-induction-based wind plant control using an engineering and a high-order wind plant model. *Wind Energy*, 19(6):1135–1150, 2016. https://doi.org/10.1002/we.1891
17. Jean Gonzalez Silva, Riccardo Ferrari, and Jan-Willem van Wingerden. Wind farm control for wake-loss compensation, thrust balancing and load-limiting of turbines. *Renewable Energy*, 203:421–433, 2023. ISSN 0960-1481. https://doi.org/10.1016/j.renene.2022.11.113
18. Daan van der Hoek, Stoyan Kanev, Julian Allin, David Bieniek, and Niko Mittelmeier. Effects of axial induction control on wind farm energy production - a field test. *Renewable Energy*, 140:994–1003, 2019. ISSN 0960-1481. https://doi.org/10.1016/j.renene.2019.03.117
19. Fleming P, King J, Simley E, Roadman J, Scholbrock A, Murphy P, Lundquist JK, Moriarty P, Fleming K, van Dam J, Bay C, Mudafort R, Jager D, Skopek J, Scott M, Ryan B, Guernsey C, Brake D (2020) Continued results from a field campaign of wake steering applied at a commercial wind farm - part 2. Wind Energy Science 5(3):945–958, https://doi.org/10.5194/wes-5-945-2020. URL https://wes.copernicus.org/articles/5/945/2020/ URL https://wes.copernicus.org/articles/5/945/2020/
20. Jan Willem van Wingerden, Lucy Pao, Jacob Aho, and Paul Fleming. Active power control of waked wind farms. *IFAC-PapersOnLine*, 50(1):4484 – 4491, 2017. ISSN 2405-8963. https://doi.org/10.1016/j.ifacol.2017.08.378. 20th IFAC World Congress
21. Paul Fleming, Jake Aho, Pieter Gebraad, Lucy Pao, and Yingchen Zhang. Computational fluid dynamics simulation study of active power control in wind plants. *2016 American Control Conference (ACC)*, pages 1413–1420, 2016. https://doi.org/10.1109/ACC.2016.7525115
22. Fele Filiberto, Maestre Jose M, Camacho Eduardo F (2017) Coalitional control: Cooperative game theory and control. IEEE Control Systems Magazine 37(1):53–69. https://doi.org/10.1109/MCS.2016.2621465
23. Sara Siniscalchi-Minna, Fernando D. Bianchi, Carlos Ocampo-Martinez, Jose Luis Domínguez-García, and Bart De Schutter. A non-centralized predictive control strategy for wind farm active power control: A wake-based partitioning approach. *Renewable Energy*, 150:656–669, 2020. ISSN 0960-1481. https://doi.org/10.1016/j.renene.2019.12.139 Jose Luis Domínguez-García, and Bart De Schutter. A non-centralized predictive control strategy for wind farm active power control: A wake-based partitioning approach. *Renewable Energy*, 150:656–669, 2020. ISSN 0960-1481. https://doi.org/10.1016/j.renene.2019.12.139
24. Dylan Wald, Jennifer King, Christopher J. Bay, Rohit Chintala, and Kathryn Johnson. Integration of distributed controllers: Power reference tracking through charging station and building coordination. *Applied Energy*, 314:118753, 2022. ISSN 0306-2619. https://doi.org/10.1016/j.apenergy.2022.118753
25. Vitor N. Coelho, Miri Weiss Cohen, Igor M. Coelho, Nian Liu, and Frederico Gadelha Guimarães. Multi-agent systems applied for energy systems integration: State-of-the-art applications and trends in microgrids. *Applied Energy*, 187:820–832, 2017. ISSN 0306-2619. https://doi.org/10.1016/j.apenergy.2016.10.056
26. Mojtaba Jabbari Ghadi, Amin Rajabi, Sahand Ghavidel, Ali Azizivahed, Li Li, and Jiangfeng Zhang. From active distribution systems to decentralized microgrids: A review on regulations and planning approaches based on operational factors. *Applied Energy*, 253:113543, 2019. ISSN 0306-2619. https://doi.org/10.1016/j.apenergy.2019.113543
27. Hao Liang, Bong Jun Choi, Weihua Zhuang, and Xuemin Shen. Stability enhancement of decentralized inverter control through wireless communications in microgrids. *IEEE Transactions on Smart Grid*, 4(1):321–331, 2013. https://doi.org/10.1109/TSG.2012.2226064
28. Dörfler Florian, Jovanović Mihailo R, Chertkov Michael, Bullo Francesco (2014) Sparsity-promoting optimal wide-area control of power networks. IEEE Transactions on Power Systems 29(5):2281–2291. https://doi.org/10.1109/TPWRS.2014.2304465
29. Christopher J. Bay, Rohit Chintala, Venkatesh Chinde, and Jennifer King. Distributed model predictive control for coordinated, grid-interactive buildings. *Applied Energy*, 312:118612, 2022. ISSN 0306-2619. https://doi.org/10.1016/j.apenergy.2022.118612

30. Hawas Yaser E, Mahmassani Hani S (1996) Comparative analysis of robustness of centralized and distributed network route control systems in incident situations. Transportation Research Record 1537(1):83–90. https://doi.org/10.1177/0361198196153700112
31. Twan Keijzer and Riccardo M.G. Ferrari. Threshold design for fault detection with first order sliding mode observers. *Automatica*, 146:110600, 2022. ISSN 0005-1098. https://doi.org/10.1016/j.automatica.2022.110600
32. Marden Jason R, Ruben Shalom D, Pao Lucy Y (2013) A model-free approach to wind farm control using game theoretic methods. IEEE Transactions on Control Systems Technology 21(4):1207–1214. https://doi.org/10.1109/TCST.2013.2257780
33. Gebraad PMO, van Wingerden JW (2015) Maximum power-point tracking control for wind farms. Wind Energy 18(3):429–447. https://doi.org/10.1002/we.1706
34. Jinkyoo Park and Kincho H. Law. A data-driven, cooperative wind farm control to maximize the total power production. *Applied Energy*, 165:151–165, 2016. ISSN 0306-2619. https://doi.org/10.1016/j.apenergy.2015.11.064
35. Zhen Dong, Zhongguo Li, Zhongchao Liang, Yiqiao Xu, and Zhengtao Ding. Distributed neural network enhanced power generation strategy of large-scale wind power plant for power expansion. *Applied Energy*, 303:117622, 2021. ISSN 0306-2619. https://doi.org/10.1016/j.apenergy.2021.117622
36. Jennifer Annoni, Christopher Bay, Kathryn Johnson, Emiliano Dall'Anese, Eliot Quon, Travis Kemper, and Paul Fleming. A framework for autonomous wind farms: wind direction consensus. *Wind Energy Science Discussions*, pages 1–17, 10 2018. https://doi.org/10.5194/wes-2018-60
37. Federico Bernardoni, Umberto Ciri, Mario A. Rotea, and Stefano Leonardi. Identification of wind turbine clusters for effective real time yaw control optimization. *Journal of Renewable and Sustainable Energy*, 13(4), 07 2021. ISSN 1941-7012. https://doi.org/10.1063/5.0036640. URL https://doi.org/10.1063/5.0036640
38. Hamed M. Al-Rahmani and Gene F. Franklin. Multirate control: A new approach. *Automatica*, 28(1):35–44, 1992. ISSN 0005-1098. https://doi.org/10.1016/0005-1098(92)90005-Z
39. M. Tomizuka. Multi-rate control for motion control applications. In *The 8th IEEE International Workshop on Advanced Motion Control, 2004. AMC '04.*, pages 21–29, 2004. https://doi.org/10.1109/AMC.2004.1297635
40. A. Jadbabaie, Jie Lin, and A.S. Morse. Coordination of groups of mobile autonomous agents using nearest neighbor rules. *IEEE Transactions on Automatic Control*, 48(6):988–1001, 2003. https://doi.org/10.1109/TAC.2003.812781
41. Reza Olfati-Saber, J. Alex Fax, and Richard M. Murray. Consensus and cooperation in networked multi-agent systems. *Proceedings of the IEEE*, 95(1):215–233, 2007. https://doi.org/10.1109/JPROC.2006.887293
42. Dörfler Florian, Simpson-Porco John W, Bullo Francesco (2016) Breaking the hierarchy: Distributed control and economic optimality in microgrids. IEEE Transactions on Control of Network Systems 3(3):241–253. https://doi.org/10.1109/TCNS.2015.2459391
43. Xiaofan Wu, Florian Dörfler, and Mihailo R. JovanoviÄ?. Topology identification and design of distributed integral action in power networks. In *2016 American Control Conference (ACC)*, pages 5921–5926, 2016. https://doi.org/10.1109/ACC.2016.7526598
44. John W. Simpson-Porco, Florian Dörfler, and Francesco Bullo. Synchronization and power sharing for droop-controlled inverters in islanded microgrids. *Automatica*, 49(9):2603–2611, 2013. ISSN 0005-1098. https://doi.org/10.1016/j.automatica.2013.05.018
45. Alvarez-Ramirez Jose, Morales America, Cervantes Ilse (1998) Robust proportional- integral control. Industrial & engineering chemistry research 37(12):4740–4747
46. Zhong-Ping Jiang and I. Marcels. Robust nonlinear integral control. *IEEE Transactions on Automatic Control*, 46(8):1336–1342, 2001. https://doi.org/10.1109/9.940947
47. Jean Gonzalez Silva, Bart Matthijs Doekemeijer, Riccardo Ferrari, and Jan-Willem van Wingerden. Active power control of wind farms: an instantaneous approach on waked conditions. *Journal of Physics: Conference Series*, 2265(2):022056, 2022. ISSN 1742-6588. https://doi.org/10.1088/1742-6596/2265/2/022056

48. Lin Xiao and Stephen Boyd. Fast linear iterations for distributed averaging. *Systems & Control Letters*, 53(1):65–78, 2004. ISSN 0167-6911. https://doi.org/10.1016/j.sysconle.2004.02.022
49. E.I. Jury. *Theory and Applications of the Z-Transform Method*. New York, 1964
50. Jury EI (1962) A simplified stability criterion for linear discrete systems. Proceedings of the IRE 50(6):1493–1500. https://doi.org/10.1109/JRPROC.1962.288193
51. Martin Andreasson, Dimos V. Dimarogonas, Henrik Sandberg, and Karl Henrik Johansson. Distributed control of networked dynamical systems: Static feedback, integral action and consensus. *IEEE Transactions on Automatic Control*, 59(7):1750–1764, 2014. https://doi.org/10.1109/TAC.2014.2309281
52. J.C. Doyle, B.A. Francis, and A. Tannenbaum. *Feedback Control Theory*. Macmillan Publishing Company, 1992. ISBN 9780023300110
53. Data-Driven Control (TU Delft). SOWFA, 2020. URL https://github.com/TUDelft-DataDrivenControl/SOWFA. Accessed: 2022-08-17
54. Søren Juhl Andersen, Ander Madariaga, Karl Merz, Johan Meyers, Wim Munters, and Carlos Rodriguez. Reference wind power plant. https://orbit.dtu.dk/en/publications/reference-wind-power-plant-d103, 2018. Tech. Rep. TotalControl Deliverable D1.3. Accessed: 2022-08-17
55. Johannes Schiffer, Florian Dörfler, and Emilia Fridman. Robustness of distributed averaging control in power systems: Time delays & dynamic communication topology. *Automatica*, 80:261–271, 2017. ISSN 0005-1098. https://doi.org/10.1016/j.automatica.2017.02.040